

The Detectability and Characterization of the TRAPPIST-1 Exoplanet Atmospheres with JWST

JACOB LUSTIG-YAEGER,^{1,2} VICTORIA S. MEADOWS,^{1,2} AND ANDREW P. LINCOWSKI^{1,2}

¹*Department of Astronomy and Astrobiology Program, University of Washington, Box 351580, Seattle, Washington 98195, USA*

²*NASA NExSS Virtual Planetary Laboratory, Box 351580, University of Washington, Seattle, Washington 98195, USA*

ABSTRACT

The James Webb Space Telescope (JWST) will offer the first opportunity to characterize terrestrial exoplanets with sufficient precision to identify high mean molecular weight atmospheres, and TRAPPIST-1's seven known transiting Earth-sized planets are particularly favorable targets. To assist community preparations for JWST observations, we use simulations of plausible post-ocean-loss and habitable environments for the TRAPPIST-1 exoplanets, and test simulations of all bright object time series spectroscopy modes and all MIRI photometry filters to determine optimal observing strategies for atmospheric detection and characterization using both transmission and emission observations. We find that transmission spectroscopy with NIRSpec Prism is optimal for detecting terrestrial, CO₂ containing atmospheres, potentially in fewer than 10 transits for all seven TRAPPIST-1 planets, if they lack high altitude aerosols. If the TRAPPIST-1 planets possess Venus-like H₂SO₄ aerosols, up to 12 times more transits may be required to detect an atmosphere. We present optimal instruments and observing modes for the detection of individual molecular species in a given terrestrial atmosphere and an observational strategy for discriminating between evolutionary states. We find that water may be prohibitively difficult to detect in both Venus-like and habitable atmospheres due to its presence lower in the atmosphere where transmission spectra are less sensitive. Although the presence of biogenic O₂ and O₃ will be extremely challenging to detect, abiotically produced oxygen from past ocean loss may be detectable for all seven TRAPPIST-1 planets via O₂-O₂ collisionally-induced absorption at 1.06 and 1.27 μm , or via NIR O₃ features for the outer three planets. Our results constitute a suite of hypotheses on the nature and detectability of highly-evolved terrestrial exoplanet atmospheres that may be tested with JWST.

Keywords: planets and satellites: atmospheres – planets and satellites: individual (TRAPPIST-1) – planets and satellites: terrestrial planets – techniques: spectroscopic

1. INTRODUCTION

The discovery of Earth-sized planets in temperate orbits around nearby, low-mass stars opens a new door into the era of terrestrial exoplanet atmospheric characterization (Berta-Thompson et al. 2015; Anglada-Escudé et al. 2016; Gillon et al. 2016, 2017; Luger et al. 2017b; Dittmann et al. 2017). Transmission and emission (secondary eclipse) spectroscopy of transiting rocky worlds with the upcoming James Webb Space Telescope (JWST) may offer a first glimpse into the atmospheres of terrestrial exoplanets (Morley et al. 2017; Kalirai 2018) and a first opportunity to search for signs of habitabil-

ity (Lincowski et al. 2018) and biosignatures beyond the Solar System (Cowan et al. 2015).

The TRAPPIST-1 system of seven transiting Earth-sized exoplanets (Gillon et al. 2016, 2017; Luger et al. 2017b) is observationally favorable for the atmospheric characterization of small exoplanets. TRAPPIST-1 is a late M dwarf (M8V; Liebert & Gizis 2006) with a small radius (0.121R_⊙; Van Grootel et al. 2018), which increases planetary transit and eclipse depths; it has a low effective temperature (2511 K; Van Grootel et al. 2018), which increases the eclipse depth; and it is nearby to Earth (12.2 pc; Gillon et al. 2016). These system properties increase sensitivity to atmospheric spectral features in transmission and emission spectroscopy, particularly for small, temperate planets.

Observations of the TRAPPIST-1 planets with the *Kepler*, *Hubble* (HST), and *Spitzer* space telescopes sug-

gest that the innermost 6 planets do not have primordial, low mean molecular weight atmospheres, but whether they have high molecular weight atmospheres or no atmospheres at all requires observations with future facilities. HST Wide Field Camera 3 (WFC3) transmission spectroscopy has ruled out H₂-dominated atmospheres for most of the TRAPPIST-1 planets (de Wit et al. 2016, 2018), and instead they may have secondary outgassed atmospheres composed of relatively high mean molecular weight gases (Moran et al. 2018). Secondary atmospheres are more difficult to detect—or rule out—than primordial atmospheres, and they may span a large range in temperature, pressure, and composition. Consequently a broad variety of potential atmospheres are consistent with the current modest observational constraints (Delrez et al. 2018; Lincowski et al. 2018).

Alternatively, the planets could have no atmospheres, although outgassing from the possibly high-volatile-content interiors of the TRAPPIST-1 planets may make that outcome less likely. Simulations suggest that the TRAPPIST-1 planets could have had their atmospheres completely stripped (e.g. Dong et al. 2018; Airapetian et al. 2017; Roettenbacher & Kane 2017), although some models of M dwarf planets suggest that atmospheric loss rates may be less than the replenishment rate via outgassing from a planetary interior (Garcia-Sage et al. 2017; Bolmont et al. 2017), such that atmospheres may be retained. The TRAPPIST-1 planets may also have larger volatile reservoirs than Solar System terrestrials. Masses derived from transit timing variation (TTV) analyses of *Kepler* (Grimm et al. 2018) and *Spitzer* observations (Delrez et al. 2018) suggest that the planets have densities between 0.6 to 1.0 ρ_{\oplus} , consistent with a rocky composition with a significant fraction of ices (Grimm et al. 2018). This conclusion is supported by the resonant chain structure of the TRAPPIST-1 system, which suggests inward migration from more volatile-rich formation orbits (Luger et al. 2017b). Determining whether the interplay of planetary processes over time will allow M dwarf terrestrial planets to maintain high-molecular weight atmospheres and support habitability will be key science questions for JWST.

Previous simulations have demonstrated the plausibility of detecting terrestrial atmospheres with JWST for M dwarf planetary systems in general (e.g. Belu et al. 2011; Barstow et al. 2016), and for the TRAPPIST-1 planets in particular (Barstow & Irwin 2016; Morley et al. 2017; Batalha et al. 2018; Krissansen-Totton et al. 2018). Morley et al. (2017) considered Venus-like, Earth-like, and Titan-like atmospheres in thermochemical equilibrium and found that CO₂-dominated atmospheres could be detected for 6 of the 7 TRAPPIST-

1 planets in fewer than 20 transits with JWST NIRSpec/G235M, and secondary eclipse photometry with JWST/MIRI could readily detect thermal emission from TRAPPIST-1 b and c, and possibly d, e, and f. Batalha et al. (2018) investigated optimal strategies for JWST observations of the TRAPPIST-1 system and found that allowing the NIRSpec Prism to slightly saturate at the peak of the stellar spectral energy distribution (SED) could allow the dominant absorber to be detected in 10 transits of H₂O, CO₂, and N₂ dominated atmospheres. Krissansen-Totton et al. (2018) investigated the potential detectability of anoxic biosignatures in the atmosphere of TRAPPIST-1 e and concluded that 10 transits observed with JWST NIRSpec Prism may be sufficient to detect CO₂ and constrain the CH₄ abundance enough to rule out non-biological CH₄ production. Recently, Wunderlich et al. (2019) considered the detectability of photochemically self-consistent Earth-like planets in the habitable zone of various M dwarfs spectral types, including TRAPPIST-1, and found that H₂O, CH₄, and CO₂ may be detectable in ~ 10 transits with JWST. However, this study did not consider non Earth-like planetary compositions, or the effect of clouds and hazes.

These previous simulations of TRAPPIST-1 planetary atmospheres did not include photochemical forcing by the late M dwarf SED on multiple plausible planetary environments, both habitable and uninhabitable. Photochemistry can have significant impacts on terrestrial atmospheric composition (Segura et al. 2005; Rugheimer et al. 2015) and haze formation (Arney et al. 2017, 2018), which can in turn modify the resultant temperature structure (Lincowski et al. 2018), impacting the predicted spectrum in both transmission and emission. Models that include photochemistry and haze formation for terrestrial atmospheres will better predict the atmospheric composition, and inform the preparation and interpretation of upcoming observations with JWST (Lincowski et al. 2018).

In this paper we explore the potential for JWST to detect and characterize the TRAPPIST-1 planetary atmospheres and distinguish between model predictions for evolutionary outcomes and different atmospheric states. As input, we use the climatically and photochemically self-consistent atmospheric and spectral simulations of Lincowski et al. (2018), who used a rigorous line-by-line 1D radiative-convective-equilibrium climate model coupled with a 1D photochemical model to simulate different habitable and post-ocean-loss environments for the TRAPPIST-1 planets. The atmospheric bulk compositions considered by Lincowski et al. (2018) are motivated by the early high luminosity of late M dwarf stars (Baraffe et al. 2015) like TRAPPIST-1, which may drive

early ocean loss and the generation of tens to thousands of bars of O_2 (Luger & Barnes 2015; Bolmont et al. 2017; Meadows et al. 2018; Lincowski et al. 2018; Wordsworth et al. 2018). The final inventory of O_2 may be severely reduced by atmospheric and surface loss processes such that only a few bars of O_2 remain (Schaefer et al. 2016; Wordsworth et al. 2018). Depending on the initial water inventory, this process may have exhausted the entire planet’s water supply, leaving it desiccated, or the planet may have formed with enough water to endure such vigorous loss. For the ocean loss planets with efficient O_2 sinks and ongoing outgassing of volatiles, large quantities of CO_2 may build up, forming a Venus-like atmosphere (Meadows et al. 2018). Lincowski et al. (2018) also considered a habitable ocean world for TRAPPIST-1 e, for the scenario where it formed with an appreciable H_2 envelope, which was subsequently stripped to reveal a habitable core (Luger et al. 2015).

To understand the nature and possibly habitability of terrestrial exoplanets, we will need a systematic approach to environmental assessment that starts with the most scientifically significant and least expensive observation, and builds from there. For terrestrial planets orbiting M dwarfs, the first property to be determined is whether or not they have an atmosphere. If an atmosphere can be confirmed, then subsequent studies will focus on determining the nature of that atmosphere, and whether there are atmospheric characteristics that could discriminate between evolutionary outcomes. Finally, a deeper dive to search for signs of habitability, including the presence of an ocean (see Robinson 2018; Lustig-Yaeger et al. 2018) and biosignatures (see Schwieterman et al. 2018) may be warranted for planets whose initial characterization does not preclude habitable conditions.

Here we determine the feasibility of atmospheric characterization for the seven known TRAPPIST-1 exoplanets by first identifying optimal instrument selection and experiments to test whether or not the TRAPPIST-1 planets have atmospheres. We then determine how to best detect specific molecules as a second step of atmospheric characterization, and discriminate between different plausible climate and photochemically self-consistent atmospheres (e.g. O_2 -dominated, CO_2 -dominated; Lincowski et al. 2018) using JWST transmission and emission photometry and spectroscopy.

The different post-runaway, evolved planet atmospheres considered here are by no means a comprehensive set of evolutionary outcomes, but rather a representative subset of potential physically- and chemically-motivated atmospheres for which we can predict spectra. By understanding the detectability of spectral discriminants for the TRAPPIST-1 planets we develop informed

hypotheses on the nature of these planets that may later be tested with JWST observations.

The structure of the paper is as follows: In §2 we present the models and methods used to simulate JWST data and find the optimal JWST modes for detecting and characterizing plausible planet compositions. We describe our results in §3, offer a discussion of the significance of those results in §4, and conclude in §5.

2. METHODS

In the following subsections we present our methods for assessing the detectability of different self-consistent atmospheric compositions for the seven TRAPPIST-1 planets with different instruments and observational modes available to JWST. We first describe the JWST noise models used in this work (§2.1), which include a MIRI photometry component and a spectroscopy component using PandExo (Batalha et al. 2017). We then detail our model inputs (§2.2), and outline a series of experiments that can be used to successively characterize terrestrial planet environments and determine optimal observing modes (§2.3).

2.1. JWST Noise Modeling

We simulate synthetic exoplanet time-series spectroscopy and photometry with JWST to consider observations during transit (transmission) and secondary eclipse (emission). In the following two subsections we detail our modeling of JWST/MIRI photometry (§2.1.1) and JWST spectroscopy (§2.1.2).

2.1.1. JWST/MIRI Photometry

Filter photometry with JWST’s Mid-Infrared Instrument (MIRI) imager has been suggested to offer an efficient means of performing an initial characterization of Earth-sized planets around low-mass stars (Morley et al. 2017). To assess MIRI photometry, we develop a basic MIRI imaging noise model for exoplanet transit and secondary eclipse observations.

The number of photons from the planet incident upon the detector is

$$N_p = T_{\text{exp}} \frac{F_p \mathcal{T} A \lambda \Delta \lambda}{hc} \quad (1)$$

where T_{exp} is the exposure time, F_p is the spectral flux density (e.g. $W/m^2/\mu m$) from the planet, \mathcal{T} is the filter throughput, A is the telescope collecting area ($25 m^2$), λ is wavelength, $\Delta \lambda$ is the width of the wavelength bin, h is Planck’s constant, and c is the speed of light. Note that the exposure time used in our photometry model is discretized in terms of the simulated planet’s transit duration, but does not explicitly depend on the

MIRI integration times or number of groups per integration, as our time-series spectroscopy noise modeling with **PandExo** does. Photon conversion efficiency curves for the MIRI imager were acquired online¹ (Glasse et al. 2015). Photons from the star are calculated analogously using Equation 1 by replacing the planet flux with the stellar flux.

The signal-to-noise (SNR) ratio on the transit depth is given by

$$\text{SNR}_T = \frac{N_s(R_p/R_s)^2}{\sqrt{(N_s + N_{bg})/n_{\text{out}} + N_{bg} + N_s[1 - (R_p/R_s)^2]}}. \quad (2)$$

where N_s is the number of photons from the star, N_{bg} is the number of photons from background sources, and n_{out} is the number of out-of-transit transit durations observed. Background photon noise is calculated using the seven component grey-body model of Glasse et al. (2015), which includes telescope thermal and scattered zodiacal noise contributions. The SNR on the photons detected from a planet observed in secondary eclipse is given by

$$\text{SNR}_E = \frac{N_p}{\sqrt{(N_p + N_s + N_{bg})/n_{\text{out}} + N_s + N_{bg}}}. \quad (3)$$

where N_p is the number of photons from the planet. Derivations of Equations 2 and 3 are provided in Appendix A.

Saturation must be considered when planning long exposures necessary to characterize small exoplanets around nearby stars. Using the bright source limits of Glasse et al. (2015) we find that TRAPPIST-1 will saturate MIRI in the two shortest wavelength filters, F560W and F770W, for the shortest exposures allowed in the standard imaging mode. Although these shorter wavelength filters may saturate, we nonetheless consider MIRI photometry in all nine filters (F560W, F770W, F1000W, F1130W, F1280W, F1500W, F1800W, F2100W, and F2550W) to assess the atmospheric information contained in each.

2.1.2. JWST Spectroscopy

We use the JWST time-series spectroscopy simulator **PandExo**² (version 1.1.2; Batalha et al. 2017; Batalha et al. 2018) to model different observing modes and their associated noise sources for transmission and emission spectroscopy. **PandExo** leverages the core of the Space Telescope Science Institute’s Exposure Time Calculator,

Pandemia³ (version 1.2.2; Pontoppidan et al. 2016), to calculate 3-D data cubes for realistic PSF modeling. We refer the reader to Batalha et al. (2017) for a thorough description of the model and its bench-marking.

We consider a broad variety of JWST instruments and modes that are capable of exoplanet transmission and emission spectroscopy and available using **PandExo**. We include the Near-Infrared Camera (NIRCam; Greene et al. 2007, 2017) using the grism time-series mode; the Near-Infrared Spectrograph (NIRSpec; Bagnasco et al. 2007; Ferruit et al. 2014); the Near Infrared Imager and Slitless Spectrograph (NIRISS; Doyon et al. 2012) using the single object slitless spectroscopy (SOSS) mode; and the Mid-Infrared Instrument (MIRI; Bouchet et al. 2015) low resolution spectrometer (LRS; Kendrew et al. 2015).

Table 1 summarizes the different JWST instruments and modes used to simulate transmission and emission spectroscopy of the TRAPPIST-1 system. Specifically, Table 1 lists the instrument, mode, disperser, filter, subarray, read mode, wavelength range, and nominal spectral resolving power used in our **PandExo** calculations. Table 1 also presents the number of groups per integration, the observing efficiency, and the number of saturated pixels at the end of the ramp for our simulated observations of the TRAPPIST-1 system with each instrument. We use the NIRSpec Prism in three configurations. First, we use the SUB512 subarray (frame time: 0.226 s) with 2 groups per integration set by **PandExo** to avoid pixel saturation. Second, we use the SUB512s subarray (frame time: 0.144 s) with 3 groups per integration, again set by **PandExo**. Finally, we simulate a partial saturation strategy by using the SUB512 and SUB512s subarrays with 6 groups per integration to allow for slight pixel saturation near the peak of the SED (Batalha et al. 2018). This modification improves the duty cycle from 33.3% (50%) to 71.4% for the SUB512 (SUB512s) subarray, as shown in Table 1 (see “Efficiency” column). We refer to this partially saturated NIRSpec Prism mode as “NIRSpec Prism*” hereafter.

2.2. Noise Model Inputs

For the stellar input to the **PandExo** noise model, we approximate the TRAPPIST-1 stellar spectrum, which has yet to be observed, using a PHOENIX stellar model (Husser et al. 2013) with an effective temperature of $T = 2511$ K, metallicity of $[\text{Fe}/\text{H}] = 0.04$, and surface gravity $\log g = 5.23$ (Delrez et al. 2018), normalized to the K band magnitude of TRAPPIST-1 ($K = 10.30$; Grimm et al. 2018). However, we ignore the effects of stellar

¹ <http://ircamera.as.arizona.edu/MIRI/pces.htm>

² <https://natashabatalha.github.io/PandExo/>

³ <https://jwst.etc.stsci.edu/>

Table 1. JWST instruments used in this study and their observability of TRAPPIST-1

Instrument	Mode	Disperser	Filter	Subarray	Read Mode	λ [μm]	R [$\lambda/\Delta\lambda$]	TRAPPIST-1		
								N_{groups}	Efficiency	N_{sat}
NIRCam	ssgrism	grism R	f322w2	subgrism64	rapid	2.42 – 4.15	~ 1600	303	99.34%	0
NIRCam	ssgrism	grism R	f444w	subgrism64	rapid	3.70 – 5.00	~ 1600	342	99.42%	0
NIRISS	SOSS	gr700xd	None	substrip96	nisrapid	0.6 – 2.8	~ 700	52	96.23%	0
NIRISS	SOSS	gr700xd	None	substrip256	nisrapid	0.6 – 2.8	~ 700	21	90.91%	0
NIRSpec	fixed slit	g140h	f100lp	sub2048	nrsrapid	0.97 – 1.82	~ 2700	39	95.00%	0
NIRSpec	fixed slit	g140m	f100lp	sub2048	nrsrapid	0.97 – 1.84	~ 1000	14	86.67%	0
NIRSpec	fixed slit	g235h	f170lp	sub2048	nrsrapid	1.66 – 3.05	~ 2700	41	95.24%	0
NIRSpec	fixed slit	g235m	f170lp	sub2048	nrsrapid	1.66 – 3.07	~ 1000	14	86.67%	0
NIRSpec	fixed slit	g395h	f290lp	sub2048	nrsrapid	2.87 – 5.14	~ 2700	82	97.59%	0
NIRSpec	fixed slit	g395m	f290lp	sub2048	nrsrapid	2.87 – 5.10	~ 1000	29	93.33%	0
NIRSpec	fixed slit	prism	clear	sub512	nrsrapid	0.6 – 5.3	~ 100	2	33.33%	0
NIRSpec	fixed slit	prism	clear	sub512s	nrsrapid	0.6 – 5.4	~ 100	3	50.00%	0
NIRSpec	fixed slit	prism	clear	sub512	nrsrapid	0.6 – 5.5	~ 100	6	71.43%	47
NIRSpec	fixed slit	prism	clear	sub512s	nrsrapid	0.6 – 5.6	~ 100	6	71.43%	19
MIRI	LRS	p750l	None	slitlessprism	fast	0.5 – 12.0	~ 100	139	98.57%	0

NOTE— N_{groups} is the number of groups per integration and N_{sat} is the number of saturated pixels at the end of the ramp. The right three columns are outputs from the **PandExo** JWST noise model specifically for observations of the TRAPPIST-1 system.

opacity in the MIR, stellar variability due to rotation and flaring during periods of observation (Vida et al. 2017; Morris et al. 2018), and heterogeneous stellar photospheres (Rackham et al. 2018; Zhang et al. 2018).

We use the modeled transmission and emission spectra of Lincowski et al. (2018) as inputs into the noise models to assess the detectability of photochemically and climatically self-consistent TRAPPIST-1 planet’s atmospheres. The climate model developed by Robinson & Crisp (2018) and Lincowski et al. (2018) uses line-by-line radiative transfer computed by the Spectral Mapping and Atmospheric Radiative Transfer (SMART) code (Meadows & Crisp 1996, developed by D. Crisp), and can generate top-of-atmosphere planetary radiances and transmission spectra (Robinson 2017) of its equilibrium climate and photochemical states. See Lincowski et al. (2018) for a thorough description of the climate and photochemical modeling and subsequent climate results. The stellar spectrum used in the optical through the MIR in Lincowski et al. (2018) is identical to the stellar spectrum used here for the JWST noise model input.

For target exposure times per transit we use the median transit durations for the TRAPPIST-1 planets from Grimm et al. (2018), and for photometry and spectroscopy noise calculations we assume that an equal amount of time is spent observing in transit/eclipse versus out of transit/eclipse. For **PandExo**, we assume saturation to be an exposure level 80% of the full well and

we impose no strict noise floor for JWST spectroscopy (c.f. Greene et al. 2016). We compute noise calculations across a grid in the number of transits/eclipses ($[1, 100]$), and then use these results to derive and report the number of transits/eclipses needed to meet specific atmospheric detection and characterization metrics, as described in the following section.

2.3. Observing Experiments

We aim to identify the optimal observing approaches for JWST to (1) detect the presence of the TRAPPIST-1 planet atmospheres, and (2) characterize the composition of the atmospheres, assuming the TRAPPIST-1 planets possess atmospheres similar in nature to the evolved atmospheres modeled in Lincowski et al. (2018). We consider an atmosphere to be detected when sufficient SNR is achieved on *any* spectral feature in a transmission or emission spectrum. For atmospheric characterization, we consider a specific molecule in the atmosphere to be detected when sufficient SNR is attained on the contribution to the spectrum from that molecule, which may include multiple bands from a given molecule. Next, we detail our SNR approach for ruling out a fiducial spectrum, and then describe how the method is used to quantify the detectability of atmospheres and specific molecules within them.

2.3.1. SNR Approach

We now define a signal-to-noise ratio approach to determine the confidence with which we can rule out that our data match a fiducial transmission or emission spectrum—which is a featureless spectrum for the case of detecting atmospheres.

For each atmospheric model and JWST instrument considered, we employ the following procedure for both transit and secondary eclipse geometries. First, we run the PandExo JWST noise model across a grid in number of transits/eclipses (n_{occ}) from 1-100, which is sufficient to establish a simple SNR scaling relationship. Second, we determine the signal-to-noise on the difference between the model spectrum and the fiducial spectrum, and calculate the total expected signal-to-noise $\langle \text{SNR} \rangle$ (defined below) by summing this difference over wavelength. Finally, we solve for number of transits/eclipses, n_{occ} , such that a given $\langle \text{SNR} \rangle$ is achieved.

We define the total expected signal-to-noise using a $\Delta\chi^2$ test formalism, which is common for model selection applications. For many random drawings of synthetic data with Gaussian noise, the expected value for $\Delta\chi^2$ between two models (m_1 and m_2) is simply

$$\langle \Delta\chi^2 \rangle = \sum_{i=1}^{N_\lambda} \left(\frac{m_{1,i} - m_{2,i}}{\sigma_i} \right)^2 \quad (4)$$

assuming that the observations with uncertainties σ are truly sampled from one of the models (m_1 in this case), and where the sum is over all N_λ spectral elements for a particular instrument. Gaussian noise is not added to the synthetic spectra both to speed up calculation of the mean result, and to avoid any single random data realization from biasing our results (e.g. Feng et al. 2018). The numerator in the sum in Equation 4 is the “signal” used to discriminate between the two models, while the denominator is the “noise” on the observations. For convenience, we define

$$\text{SNR}_i = \frac{m_{1,i} - m_{2,i}}{\sigma_i}, \quad (5)$$

which is the individual signal-to-noise contribution from each spectral element to model m_2 being ruled out in favor of model m_1 . Equation 4 may then be rewritten in terms of SNR_i and what we refer to as the total expected signal-to-noise

$$\langle \text{SNR} \rangle = \sqrt{\langle \Delta\chi^2 \rangle} = \sqrt{\sum_{i=1}^{N_\lambda} \text{SNR}_i^2}. \quad (6)$$

Equation 6 is particularly useful because the quadrature sum over wavelength allows for the comparison between multiple different JWST instruments that may have different spectral resolutions and wavelength ranges, and

for a comparison between transmission and emission spectroscopy for the same hypothesis (e.g. *the planet does not have an atmosphere*).

We caution that Equation 6 is equal to the confidence in the detection of model m_1 in units of standard deviations (number of “sigma” n_σ), only in the case that each model has one degree of freedom. To avoid assumptions on the degrees of freedom and degeneracies associated with spectral models, we simply report $\langle \text{SNR} \rangle$ with the understanding that these are upper limits on the confidence in the detection. Furthermore, when we report the number of transits/eclipses to rule out the fiducial model to a given $\langle \text{SNR} \rangle$, these are lower limits; additional sources of uncertainty and/or retrieval model complexity may require that more transits/eclipses be observed.

We now detail the fiducial spectral models that are used to detect the presence of an atmosphere and the individual molecules with them.

2.3.2. Detecting the presence of an atmosphere

The spectra of planets with atmospheres can be discriminated from the featureless spectra of airless worlds by the presence of spectral absorption features. This approach works best for atmospheres with strong absorption features, but will be challenging for transmission spectroscopy if molecular absorption is suppressed by a high mean molecular weight atmosphere (Miller-Ricci et al. 2009), the presence of clouds and hazes (Berta et al. 2012; Ehrenreich et al. 2014; Knutson et al. 2014; Kreidberg et al. 2014; Nikolov et al. 2015), or atmospheric refraction (Bétrémieux & Kaltenegger 2014; Misra et al. 2014). In these cases, higher SNR observations will be required to detect the presence of an atmosphere. Here we assess the detectability of realistic terrestrial atmospheres with clouds and hazes in transmission by comparing their spectra to a baseline featureless spectrum that is modeled as the best-fitting constant planet radius with wavelength. For the corresponding emission spectrum test, we model the featureless spectrum as the ratio of two blackbodies at the stellar effective temperature and best-fitting planetary equilibrium temperature (set by a variable bond albedo).

While there are several “false negative” processes that could suppress the signal from an atmosphere as described above, one “false positive” process is worth considering: the possibility that surface mineralogy could produce wavelength dependent features in emission spectra of airless worlds. However, these features are unlikely to be as prominent as atmospheric features, and this is especially true in realistic cases where multiple reflections occur within the mineral surface. Specif-

ically, by Kirchoff’s law of thermal radiation, the emissivity ϵ is related to the reflectance R by (Nicodemus 1965),

$$\epsilon = 1 - R. \quad (7)$$

The emissivity then regulates the efficiency of thermally radiated flux F_λ relative to a perfect blackbody $B_\lambda(T)$ via

$$F_\lambda = \epsilon_e B_\lambda(T), \quad (8)$$

for an object with an equilibrium temperature T . However, Equation 8 uses the *effective* emissivity,

$$\epsilon_e = 1 - (1 - \epsilon)^{(n+1)}, \quad (9)$$

which accounts for the number of reflections n within the material, and ultimately decreases the contrast of mineralogical features in the thermal emission spectrum (Kirkland et al. 2003; Hu et al. 2012).

Figure 1 compares secondary eclipse spectrum models for different assumed end-member planet mineralogical compositions. Emission spectra are shown for planets at the zero bond albedo equilibrium temperature composed solely of quartz, basalt, olivine, pyroxene, hematite, anthorite, enstatite, saponite, and feldspar—a selection of common rocks and minerals found in terrestrial solar system bodies. For comparison, also shown are emission spectra with strong atmospheric absorption features from the climatically and photochemically self-consistent 100 bar O₂-dominated and 92 bar CO₂-dominated atmospheres from Lincowski et al. (2018).

In some cases, mineralogical surface emission features compare in signal contrast to model atmospheric thermal emission features, but under most plausible physical scenarios an airless rock would likely have significantly lower spectral variation than atmospheric features. The single-reflection quartz silicate features between $\sim 8 - 10 \mu\text{m}$ and $\sim 19 - 23 \mu\text{m}$ are strong and rival the strength of the atmospheric features caused by O₃, CO₂, and H₂O over this wavelength range. However, single reflections are unlikely, and both multiple reflections and blends of different minerals would decrease the contrasts on features from any one of the representative end-member cases, producing a relatively featureless thermal emission spectrum.

Throughout the rest of the paper, unless otherwise stated, we adopt the assumption that detecting deviations from blackbody emission in a secondary eclipse spectrum are evidence of an atmosphere. However, in §3 we further explore the detectability of quartz silicate emissivity features in the emission spectrum of TRAPPIST-1b observed with MIRI LRS as an optimistic limiting case on the potential signal from an airless body.

Figures 2 and 3 provide a specific example of a test for the presence of a 10-bar CO₂ atmosphere, using both transmission (with NIRSPEC Prism*) and emission (with MIRI LRS) spectroscopy, respectively. The bottom panel of each figure shows a direct comparison between the template spectrum and the featureless model that best fits the template spectrum. The color-contours show the magnitude of difference between the two spectra in the bottom panel divided by the noise ($|\text{SNR}_i|$) as a function of wavelength and number of occultations. The right panels show the total expected SNR, $\langle \text{SNR} \rangle$, as a function of number of occultations, which is the total signal of the atmosphere over the wavelength range of the instrument. The quadrature sum over wavelength not only allows for a comparison between different instruments that naturally accounts for the native resolution of and noise incurred by the instrument, but also a comparison between transmission and emission spectroscopy. Comparing Figures 2 and 3 we see that if TRAPPIST-1b possesses a 10 bar high CO₂ atmosphere, detecting that atmosphere by molecular features in the spectrum will require fewer transits with NIRSpec Prism* than secondary eclipses with MIRI LRS. This example demonstrates how we identify optimal observing modes for atmosphere detections, and enables a comprehensive study to determine the exposure times needed detect the presence of an atmosphere as a function of observing mode and atmosphere type.

Unless otherwise stated, throughout the rest of the paper we adopt the convention that an atmosphere is detected if $\langle \text{SNR} \rangle \geq 5$ is achieved on absorption features in the spectrum. We report our results for the detectability of atmospheres at this threshold, but encourage readers to scale our results to their own desired detection thresholds.

2.3.3. Detecting Specific Molecules

To detect individual molecules in the spectrum, we apply the methods described in the previous sections to spectra with and without the absorption features from a given molecular species. To perform these tests we generate additional transmission and emission spectra by running our radiative transfer model for a given atmosphere with each spectrally active molecule removed one at a time. We then use the spectra that are missing contributions from individual molecules as m_2 in Equation 4 and 6 to calculate the $\langle \text{SNR} \rangle$ on the contribution from each molecule to the spectrum. In this case, rather than a “flat line” test, where we attempt to rule out a featureless spectrum and thereby detect the presence of an atmosphere, here we attempt to rule out a spectrum that does not have a particular gas—for instance H₂O—and

TRAPPIST-1b : Airless Rocks in Eclipse

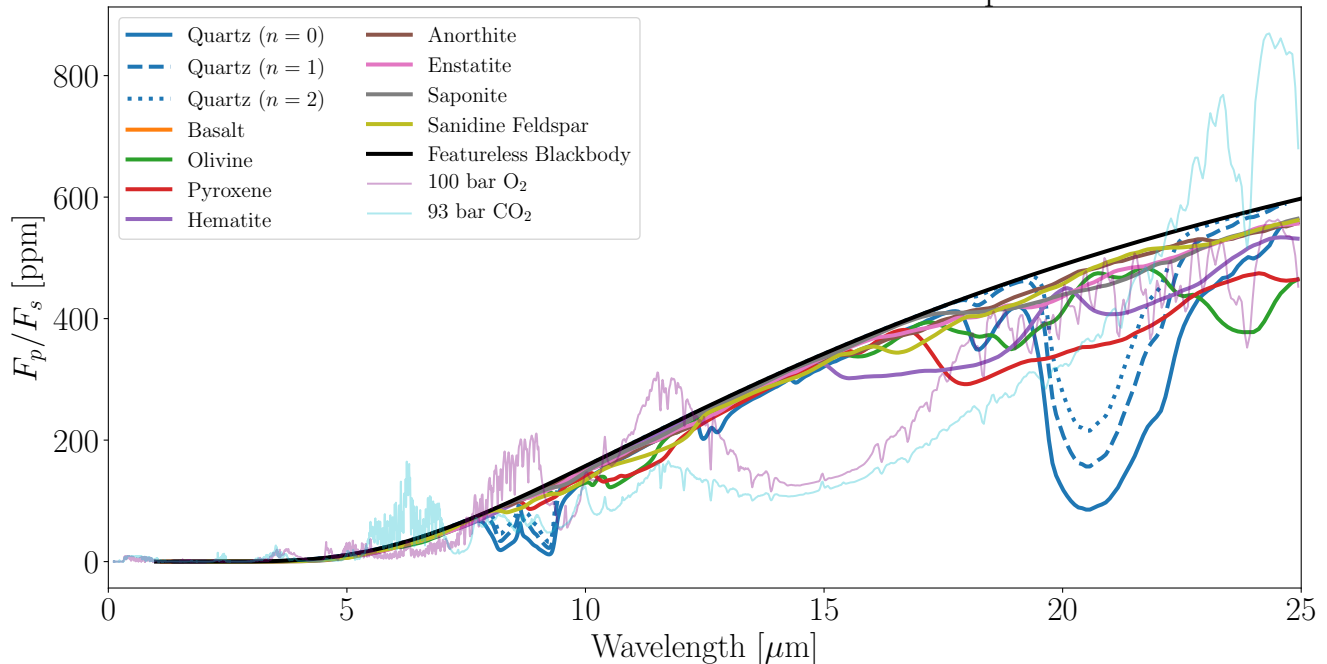


Figure 1. Secondary eclipse spectrum models of TRAPPIST-1b assuming different end-member planet mineralogical compositions. The black line shows a featureless blackbody curve, corresponding to the zero bond albedo planet equilibrium temperature, from which all of the thermal emission curves from rock forming minerals (thick color lines) deviate due to non-unity, wavelength-dependent emissivities. The three line styles for the quartz curves demonstrate the reduction in effective emissivity due to n reflections within the rock (see equation 9). The thin purple and teal lines show the expected emission spectrum for TRAPPIST-1b if it were to possess a climatically and photochemically self-consistent thick O_2 - or a CO_2 -dominated atmosphere, respectively (Lincowski et al. 2018).

thereby detect the presence of H_2O . This procedure enables the identification of which JWST instruments and modes are sensitive to detecting individual molecules in an observed spectrum and how much time must be spent on any given target to reduce the noise enough to measure the spectral contributions from each molecule.

Figure 4 shows the detectability of O_2 in the atmosphere of TRAPPIST-1b with NIRSpec G140H if the planet possesses a desiccated 10 bar O_2 atmosphere. The strong O_2 - O_2 collisionally-induced absorption (CIA) features at 1.06 and 1.27 μm lead to a $\langle SNR \rangle = 5$ detection of O_2 in 7 transits. Therefore, an oxygen dominated atmosphere for TRAPPIST-1b could be *ruled out* by not detecting these features in 7 transits.

Unless otherwise stated, throughout the rest of the paper we adopt the convention that molecules in the atmosphere are weakly detected if $\langle SNR \rangle \geq 3$ is achieved on that molecule’s contribution to the spectrum, and we report our results for the characterization of atmospheres at this weak detection threshold. Keep in mind that we use a weaker threshold $\langle SNR \rangle$ to report detecting individual molecules than for simply detecting the atmosphere, but we encourage readers to scale our molecular detection results to their own desired thresholds.

3. RESULTS

Here we present the full results of our simulations on the detectability and characterization of the TRAPPIST-1 exoplanet atmospheres using JWST. First, we assess the JWST observations needed to detect the presence of an atmosphere for the TRAPPIST-1 planets (§3.1). We then address the detectability of individual molecules within the TRAPPIST-1 planet spectra that may be used to distinguish between different atmospheric states and evolutionary scenarios (§3.2).

3.1. Detecting Atmospheres

We simulate the detectability of the TRAPPIST-1 planetary atmospheres with MIRI photometry (§3.1.1), transmission spectroscopy (§3.1.2), and emission spectroscopy (§3.1.3).

3.1.1. JWST/MIRI Photometry

MIRI photometry may be advantageous for initial assessments prior to the potentially long time commitment necessary to observe the spectrum of the Earth-sized TRAPPIST-1 planets with JWST. We investigate both transit and eclipse photometry with the nine MIRI pho-

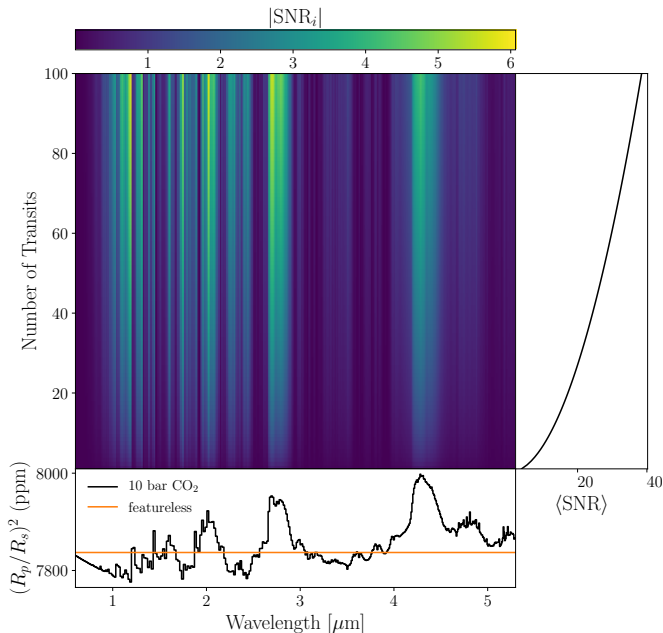


Figure 2. Signal-to-noise contours on the simulated 10 bar high CO₂ transmission spectrum, observed with JWST/NIRSpec Prism with 6 groups per integration, relative to a featureless spectrum as a function of the number of transits observed and wavelength of the instrument. The bottom panel shows the noiseless spectrum (black) and the best-fitting featureless spectrum (orange), both convolved to the instrument resolution. The right panel shows how the total expected SNR from Equation 6 increases with more transits observed.

tomeric filters spanning wavelengths from about 5 to 27 μm (Bouchet et al. 2015). We first present results that may help to constrain the presence of an atmosphere from secondary eclipse observations in a *single* MIRI photometric band using brightness temperature arguments. We then present results for transit and eclipse observations in multiple filters, using the tests described in §2.3.2, to assess the observational requirements for ruling out a featureless spectrum.

Single-Band Constraints—We calculate brightness temperatures for each of our self-consistent atmosphere models (Lincowski et al. 2018) to help plan and interpret photometric assessments of the TRAPPIST-1 planets in secondary eclipse. Figure 5 shows brightness temperature as a function of wavelength for TRAPPIST-1b for different assumed atmospheres. The wavelength-dependent fluxes were also convolved with the nine MIRI filters to calculate the brightness temperature of each atmosphere model, shown as color points in Fig. 5. The horizontal dashed line shows the zero bond albedo equilibrium temperature of TRAPPIST-1b—a limit which a planet without additional internal geothermal or at-

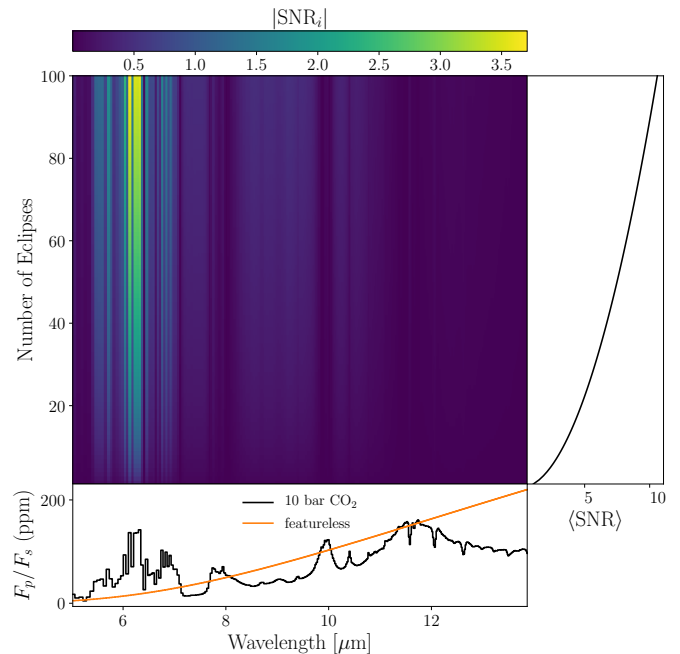


Figure 3. Signal-to-noise contours on the simulated 10 bar high CO₂ emission spectrum observed with JWST/MIRI/LRS relative to a featureless spectrum as a function of the number of occultations observed and wavelength of the instrument. The bottom panel shows the noiseless spectrum (black) and the best-fitting featureless spectrum (orange), both convolved to the instrument resolution. The right panel shows how the total expected SNR from Equation 6 increases with more eclipses observed.

mospheric greenhouse heating would not be expected to exceed. Figure 5 also provides the SNR on the depth of a single observed secondary eclipse, averaged over the atmospheric models and displayed increasing from top to bottom on the right y-axis.

A few of the possible TRAPPIST-1b atmospheres, in particular the Venus-like and outgassing O₂ atmospheres, have brightness temperatures that exceed the zero bond albedo equilibrium temperature in a handful of the MIRI photometric bands. Like Venus, the 10 and 92 bar CO₂ atmospheres have 6 μm windows that provide a glimpse into their hotter, greenhouse heated, lower atmospheres. The F560W MIRI filter could potentially detect this emission. The 10 and 100 bar O₂ outgassing atmospheres also have strong emission windows near 11.5 μm , between the 9.6 μm O₃ band and the 15 μm CO₂ band, which could be detected with the F1130W MIRI filter. The 10 and 92 bar CO₂ atmospheres have sufficiently strong CO₂ absorption to saturate the wings of the 15 μm band and cause a significantly lower brightness temperature at 10–12 μm compared to atmospheres not dominated by CO₂. The 10 and 92 bar CO₂ atmospheres also exceed the maxi-

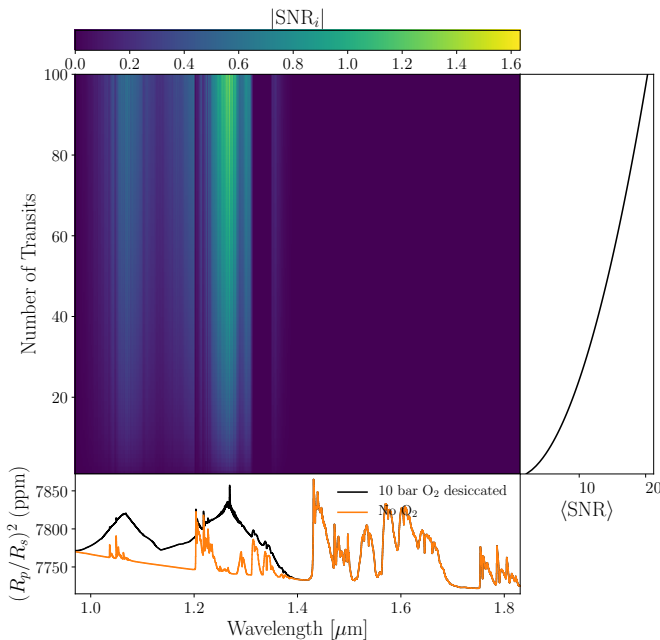


Figure 4. Signal-to-noise contours on the O_2 contribution to the transmission spectrum of TRAPPIST-1b if it possesses a 10 bar desiccated high O_2 atmosphere observed with NIRSpec G140H as a function of the number of occultations observed and wavelength of the instrument. The bottom panel shows the full model spectrum (black) and the model spectrum with O_2 removed (orange), both convolved to the resolution of NIRSpec G140H. The right panel shows the total expected SNR ($\langle \text{SNR} \rangle$) from Equation 6. The O_2 features at 1.06 and 1.27 μm are due to $\text{O}_2\text{-O}_2$ collisionally-induced absorption (CIA), and could lead to $\langle \text{SNR} \rangle = 5$ detection of O_2 in ~ 7 transits.

num equilibrium brightness temperature beyond about 22 μm , however the F2550W MIRI filter may lack the SNR to provide constraining information.

Despite the few cases with potentially detectable high brightness temperatures, the overwhelming majority of atmospheric models viewed through MIRI filters have brightness temperatures that are consistent with a plausible planetary bond albedos (between 0 and 1), including in the 12-18 μm wavelength range where outgoing thermal radiation is strongly absorbed by the broad 15 μm CO_2 band. In the atmospheres that we considered, no *single* photometric band stands out above the rest as providing a definitive detection of an atmosphere via an emission window. However, using secondary eclipse observations in multiple MIRI filters in and out of the strong 15 μm CO_2 feature may be used to detect the presence of an atmosphere. We discuss this point later in this section.

Although Figure 5 only shows brightness temperatures for TRAPPIST-1b, Table 3 in Appendix C lists the brightness temperature in each MIRI imaging filter for

each TRAPPIST-1 planet atmosphere considered here. Table 3 also contains calculations for the Warm Spitzer photometric filters. We note, however, that the SNR on secondary eclipses decreases rapidly with planet equilibrium temperature, making precise eclipse photometry beyond TRAPPIST-1c largely infeasible with JWST.

Multi-Band Constraints—We now turn to constraints that may be placed on the existence of an atmosphere using a combination of any of the nine MIRI photometric bands to observe either transits or eclipses. For each type of atmosphere, we determine the number and set of MIRI filters that can detect the atmosphere using transit and eclipse photometry in the minimum number of total occultations, assuming an equal number of occultations are observed in each filter. In all cases, 2-3 MIRI filters is optimal for detecting deviations from a featureless spectrum and additional filters are costly given their marginal increase in atmospheric detectability. The F1500W filter is always optimal to include due to the presence of CO_2 in these atmospheres. For transit photometry, the F1500W filter is best combined with F560W for CO_2 -dominated atmospheres and F770W for O_2 -dominated atmospheres, and typically just 2 filters is optimal. For eclipse photometry, the F1500W filter is best combined with F560W, F770W, and/or F1130W, and typically 3 filters is optimal.

The left panel of Fig. 6 shows the total number of transits (blue lines) and eclipses (red lines) needed to detect different atmospheric compositions for each of the seven known TRAPPIST-1 planets using the optimal 2 or 3 MIRI photometric filters. Plotting the number of occultations (transits or eclipses) as a function of the TRAPPIST-1 planets, ordered by semi-major axis, reveals a general trend according to the observation method: emission photometry is comparable with transmission photometry at detecting atmospheres for the innermost/hottest planets (e.g. TRAPPIST-1b and c), but becomes increasingly less efficient as the planets decrease in equilibrium temperature; whereas transmission photometry increases in observational time much more gradually with equilibrium temperature. This strong scaling with temperature occurs because the planet emission, at wavelengths contributing most to the detection of molecular features, is not in the Rayleigh-Jeans limit. The left panel of Fig. 6 implies that determining whether or not the potentially habitable TRAPPIST-1 planets (e, f, and g) have atmospheres will be much more efficient with transit photometry than eclipse photometry.

The high CO_2 atmospheres may be surprisingly difficult to distinguish with eclipse photometry because the wings of the 15 μm CO_2 band saturate and extend many

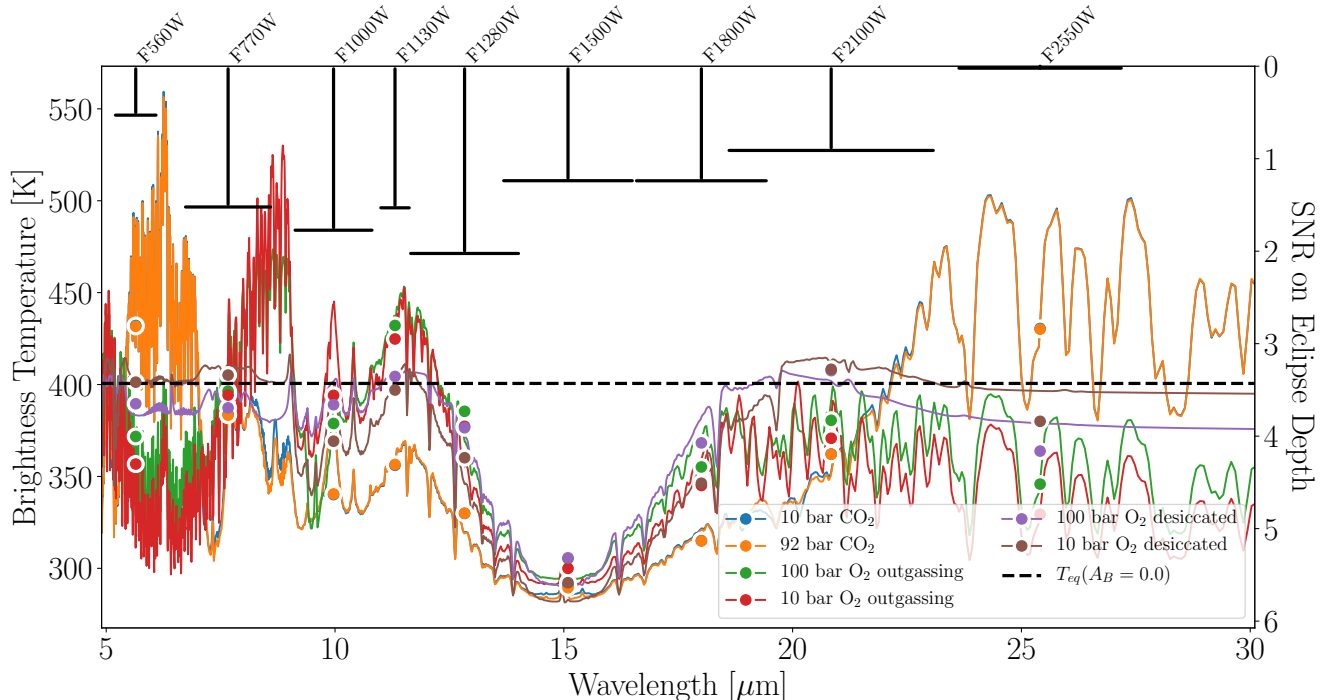


Figure 5. Brightness temperatures for different TRAPPIST-1b atmospheric models across the JWST/MIRI imaging wavelength range. The average brightness temperature integrated across each MIRI filter are shown as color points. The zero bond albedo equilibrium temperature of TRAPPIST-1b (black horizontal dashed line) is shown to compare against the model brightness temperatures, which vary as a function of wavelength due to the interplay between atmospheric temperature structure and gaseous opacities. The black lines from the top of the plot correspond to the (atmospheric model averaged) SNR on a single secondary eclipse, shown increasing from the top of the right y-axis to the bottom. These SNR indicators are shown capped with the effective width of each MIRI filter, and help to identify which filters may best offer secondary eclipse detections.

microns on either side. This strong absorption effectively mutes the planet’s emitted flux, creating a nearly featureless spectrum. Consequently, MIRI eclipse photometry at $12.8 \mu\text{m}$ and $18 \mu\text{m}$ (F1280W and F1800W filters, respectively) may not be sufficiently separated from $15 \mu\text{m}$ (F1500W) to avoid substantial contamination from the wings of strong CO_2 absorption (see the orange curve in Fig. 5), making these filters ineffective for continuum measurement. Instead, the F1130W filter may be better at probing deeper into the atmosphere.

3.1.2. JWST Transmission Spectroscopy

We now present results on the detectability of the TRAPPIST-1 planet atmospheres using transmission spectroscopy with JWST. We begin with a few specific examples of detectable TRAPPIST-1 atmospheres to demonstrate the size of molecular absorption features relative to the expected JWST noise, and then present our full ensemble of results for each TRAPPIST-1 planet, atmosphere, and JWST instrument.

Specific Examples of Atmospheric Detection—Figure 7 shows an example detection of absorption features in the transmission spectrum of TRAPPIST-1 b assuming it

possesses a clear 10 bar CO_2 atmosphere. The transmission spectrum is shown with synthetic data simulated for two transits observed with NIRSpec Prism*, which we find to be sufficient to rule out a featureless spectrum with $\langle \text{SNR} \rangle = 5$ (our fiducial detection limit). The synthetic data are shown binned to a resolution of $R = 8$, however the featureless spectrum was ruled out at the native resolution of the NIRSpec Prism ($R \approx 100$). CO_2 absorption features at $1.6, 2.0, 2.8, 4.3 \mu\text{m}$ drive the detectability of this atmosphere and are apparent in the synthetic data.

Figure 8 demonstrates possible transmission spectra of TRAPPIST-1 c for two different aerosol conditions. Both cases are CO_2 -dominated spectral models from Lincowski et al. (2018) with simulated noise for observations with NIRSpec Prism*. The number of transits observed for each model is calculated such that the atmosphere is strongly detected with $\langle \text{SNR} \rangle = 10$. The blue model shows a clear sky spectrum with large CO_2 absorption features and data uncertainties calculated for 16 observed transits. The red model includes H_2SO_4 clouds at altitudes consistent with H_2SO_4 condensation,

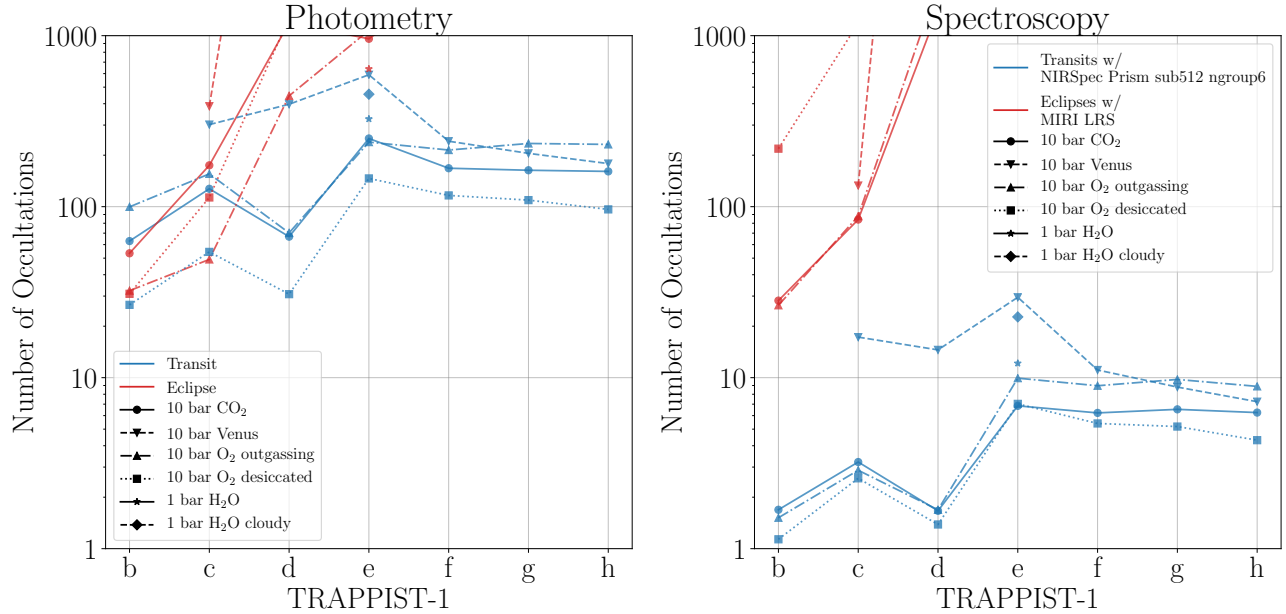


Figure 6. Number of transits (blue) or eclipses (red) needed to detect an atmosphere for all seven known TRAPPIST-1 planets with MIRI photometry (left) and JWST spectroscopy (right). Line and marker styles designate the type of atmosphere assumed. MIRI imaging assumes that the number of occultations are split evenly between the 2-3 photometric filters that are optimal to detect each atmosphere (see §3.1.1). Transmission spectroscopy is shown using NIRSpec Prism* (see §3.1.2) and emission spectroscopy is shown using MIRI LRS (see §3.1.3). Detecting the atmospheres of the TRAPPIST-1 planets is optimal using transmission spectroscopy with NIRSpec Prism across a range of terrestrial atmospheric compositions.

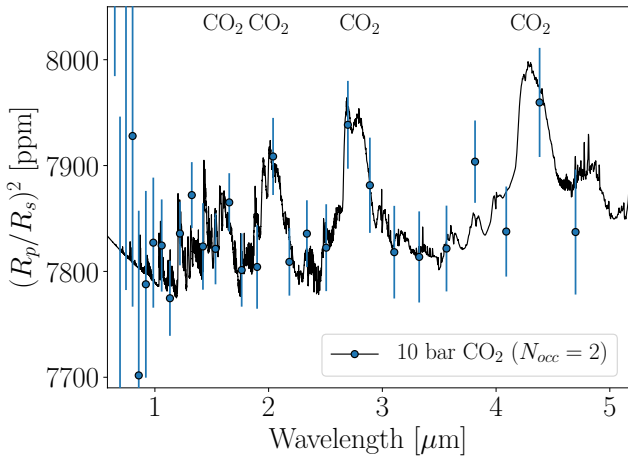


Figure 7. Model transmission spectrum of TRAPPIST-1b with a 10 bar CO₂ atmosphere. Synthetic data are simulated for two transits observed with NIRSpec Prism* and binned to a resolution of $R = 8$.

with data uncertainties calculated for 72 observed transits.

The aerosol-free atmosphere has strong CO₂ features that can be detected in considerably fewer transits than the case with Venus-like H₂SO₄ aerosols. The self-consistent clouds are located high enough in the atmosphere that over 70 transits are required to detect the CO₂ absorption features with the same confidence as

the clear sky case. If TRAPPIST-1 c possess Venus-like aerosols, then about $5\times$ more transits must be observed to achieve comparable constraints on the presence and composition of TRAPPIST-1 c’s atmosphere, than our estimates for the clear-sky case.

We find a factor of ~ 4 variation in the number of transits needed to detect the atmosphere of TRAPPIST-1e depending on the type of terrestrial atmosphere it possesses. Figure 9 explores the detectability of molecular features in the transmission spectrum of TRAPPIST-1e. Like Fig. 8, Fig. 9 shows possible TRAPPIST-1e model spectra with simulated NIRSpec Prism* observations assuming the number of transits needed to strongly detect features in each atmosphere with $\langle \text{SNR} \rangle \approx 10$. Spectra for water-covered environments with and without a water cloud are shown in teal and blue, respectively, and CO₂-dominated atmospheres, with and without H₂SO₄ aerosols are shown in orange and red, respectively. To detect features in each spectrum with $\langle \text{SNR} \rangle \approx 10$ ($\langle \text{SNR} \rangle \approx 5$), and thereby obtain approximately equal constraints on the presence of TRAPPIST-1e’s atmosphere, will require ~ 30 (~ 7) transits for a clear sky CO₂ atmosphere, ~ 50 (~ 13) transits for a clear sky aqua planet atmosphere, ~ 90 (~ 22) transits for a cloudy aqua planet atmosphere, and ~ 120 (~ 30) transits for a CO₂-dominated atmosphere with H₂SO₄ clouds.

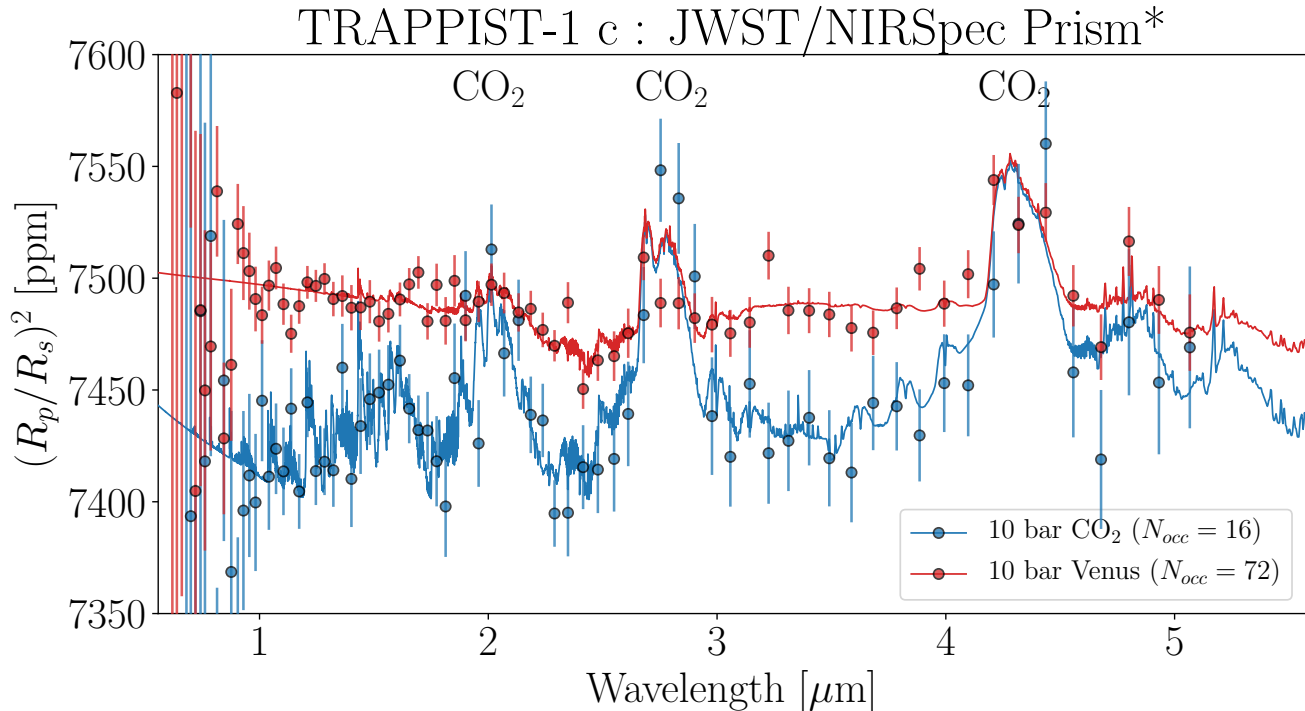


Figure 8. Simulated JWST/NIRSpec Prism transmission spectra of TRAPPIST-1c for different CO₂-dominated atmospheric states. The blue model shows a clear sky spectrum with large CO₂ absorption features and the red model includes a self-consistent H₂SO₄ cloud. The number of coadded transits simulated for each NIRSpec observation are set so that the atmosphere is strongly detected ($\langle \text{SNR} \rangle = 10$). That is, to obtain approximately equal constraints on the presence and composition of TRAPPIST-1c’s atmosphere will require 16 transits for the clear sky CO₂ case and 72 transits for the cloudy case.

Optimal JWST Observing Modes for Atmospheric Detection—Thus far we have only discussed specific cases for the detectability of the TRAPPIST-1 planet atmospheres with JWST transmission spectroscopy; we now report results from our comprehensive study to determine the exposure times needed to detect the presence of atmospheres as a function of JWST observing mode and atmosphere type, for each TRAPPIST-1 planet. The number of transits necessary to detect spectral features in the transmission spectrum with $\langle \text{SNR} \rangle = 5$ for TRAPPIST-1 b, c, d, e, f, g, and h are shown in Appendix B in Figures 13, 14, 15, 16, 17, 18, and 19, respectively, as a function of both atmospheric compositions and JWST instrument/mode. Color is used in these figures to guide the eye to small (more blue) and large (more white) values for the number of transits.

These results suggest that under most circumstances the JWST/NIRSpec Prism is the optimal instrument for detecting the presence of an atmosphere using transmission spectroscopy of the TRAPPIST-1 planets. If a partial saturation strategy is used with the NIRSpec Prism (Batalha et al. 2018), then it will be more capable of detecting atmospheric features than any other JWST instrument or mode. However, if it turns out that the systematics introduced via partial saturation are not ben-

eficial, the SUB512S subarray will offer improved performance over the SUB512 subarray due to its shorter readout time. Although we note that SUB512 should be considered the subarray of choice because SUB512s has limited access to important background pixels and it may be difficult to keep the curved trace inside only 16 pixels in the cross-dispersion direction. The NIRSpec G395M/H disperser offers comparable results with the standard (no partial saturation) NIRSpec Prism.

Most of the atmospheres that we consider may require fewer than 12 transits to detect for all of the TRAPPIST-1 planets using the optimized NIRSpec Prism mode. Figure 10 displays the number of transits to detect the TRAPPIST-1 planet atmospheres using only the NIRSpec Prism* instrument for each TRAPPIST-1 planet and for each atmosphere considered in this work.

Our results show that the outer TRAPPIST-1 planets require only 2-7 more transits than TRAPPIST-1 b to detect clear-sky atmospheres. The right panel of Fig. 6 summarizes the best-case-scenario results for detecting the atmospheres of the TRAPPIST-1 planets with JWST transit spectroscopy (blue lines). The number of transits required to detect the atmosphere at $\langle \text{SNR} \rangle = 5$ for each of the atmospheric models is shown for observa-

TRAPPIST-1 e : JWST/NIRSpec Prism*

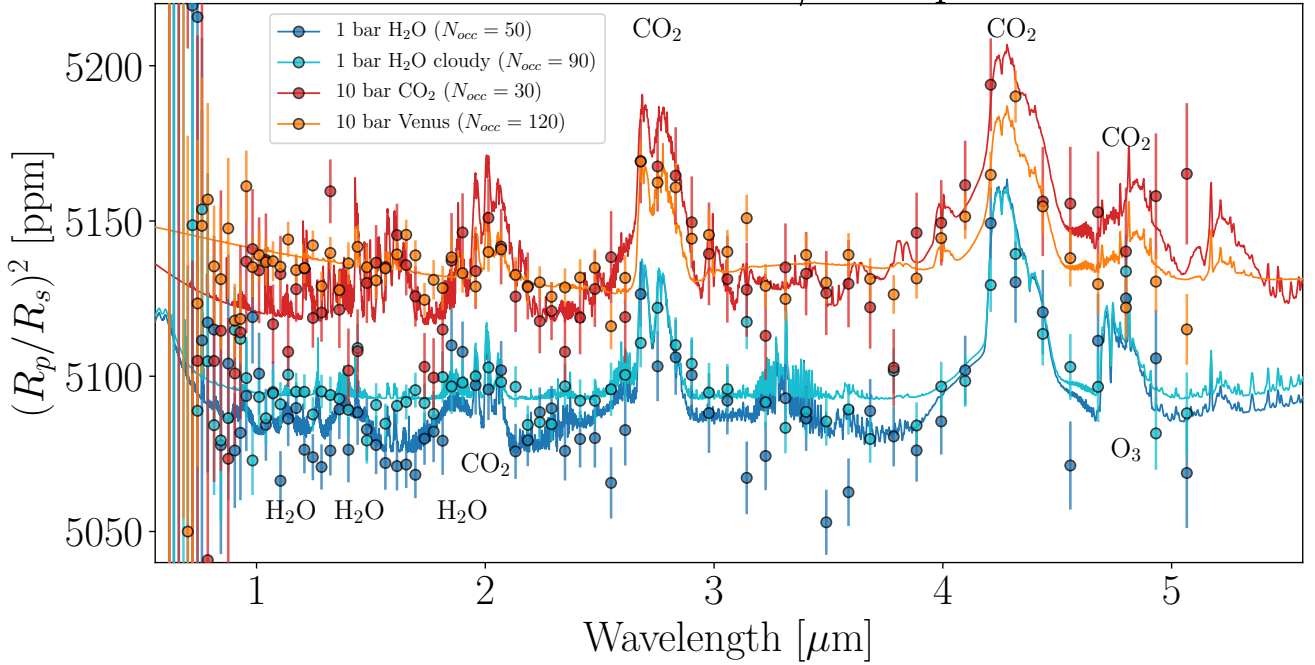


Figure 9. Simulated JWST/NIRSpec Prism* transmission spectra of TRAPPIST-1e for different possible atmospheric compositions. The teal and blue models show spectra for water-dominated atmospheres, with and without a water cloud, respectively. The orange and red spectra are for CO₂-dominated atmospheres, with and without H₂SO₄ aerosols, respectively. The number of coadded transits simulated for each NIRSpec observation are set so that the atmosphere is strongly detected ($\langle \text{SNR} \rangle = 10$). That is, to obtain approximately equal constraints on the presence of TRAPPIST-1e’s atmosphere will require ~ 30 transits for a clear sky CO₂ atmosphere, ~ 50 transits for a clear sky H₂O atmosphere, ~ 90 transits for a cloudy H₂O atmosphere, and ~ 120 transits for a CO₂-dominated Venus-like atmosphere.

tions with NIRSpec Prism*. Like our transit photometry results, the number of transits only weakly increases with semi-major axis. However, significantly fewer transits are required for transmission spectroscopy atmosphere detections with NIRSpec Prism* than with MIRI filter photometry. The emission spectroscopy results in Fig. 6 (red lines) are discussed in §3.1.3.

The atmospheric composition of the planets has a relatively minimal effect on the number of transits needed to rule out a featureless spectrum, with Venus-like clouds being a significant exception. All atmospheric cases considered for TRAPPIST-1 c could be detected in 3-4 transits with NIRSpec Prism*, except for the 10 and 92 bar Venus atmospheres (with H₂SO₄ aerosols), which would require 4.5 \times and 5.5 \times the number of transits to detect, respectively, compared to the 10 and 92 bar clear-sky CO₂ counterparts. In general, more transits tend to be required to detect the atmospheres of the cooler worlds, except for TRAPPIST-1 d, which is more comparable to TRAPPIST-1 b in the detectability of its atmosphere. While the atmosphere of TRAPPIST-1 d may be relatively easy to detect if it is without clouds, with clouds the 10 and 92 bar CO₂ atmospheres require 7.5 \times and

12 \times the number of transits to detect, respectively, the largest increase due to clouds seen in the sample. Beyond TRAPPIST-1 e the effect of Venus-like clouds has a diminished impact on the atmospheric detectability, with fewer than 2 \times the number of transits required to detect the atmospheres for TRAPPIST-1 f, g, and h if they have clouds.

Note that the numerical values in Figure 10 and Figures 13 - 19 can easily be scaled to higher or lower $\langle \text{SNR} \rangle$ thresholds that more or less confidently rule out a featureless spectrum. Since the SNR on an observation (and $\langle \text{SNR} \rangle$) scales with the square-root of the exposure time, and the number of occultations is a proxy for exposure time, we can obtain a new value for the number of occultations:

$$N'_{\text{occ}} = N_{\text{occ}} \left(\frac{\langle \text{SNR} \rangle'}{\langle \text{SNR} \rangle} \right)^2 \quad (10)$$

where N_{occ} is the number of occultations necessary to distinguish features in the spectrum with $\langle \text{SNR} \rangle$ (5 in Figures 10, 13 - 19) and $\langle \text{SNR} \rangle'$ is the new signal-to-noise threshold.

Detect Atmospheres in Transit with $\langle \text{SNR} \rangle = 5.0$
NIRSpec Prism sub512 ngroup6

Type of Atmosphere	b	c	d	e	f	g	h
1 bar H ₂ O	—	—	—	13	—	—	—
1 bar H ₂ O cloudy	—	—	—	23	—	—	—
10 bar CO ₂	2	4	2	7	7	7	7
92 bar CO ₂	2	4	2	8	7	7	7
10 bar Venuss	—	18	15	30	12	9	8
92 bar Venuss	—	22	24	31	12	11	8
10 bar O ₂ outgassing	2	3	2	10	9	10	9
100 bar O ₂ outgassing	2	4	2	7	5	4	4
10 bar O ₂ desiccated	2	3	2	8	6	6	5
100 bar O ₂ desiccated	2	4	2	11	9	8	6

TRAPPIST-1

Figure 10. Number of transits for each TRAPPIST-1 planet necessary to rule out a featureless spectrum with $\langle \text{SNR} \rangle = 5$ for different self-consistent atmospheric compositions using JWST NIRSpec Prism with the optimized readout mode of Batalha et al. (2018).

The increased transit duration with semi-major axis make our results for the outer TRAPPIST-1 planets appear more optimistic relative to our results for the inner planets. Note that for JWST planning, our reported number of transits/eclipses leads to different telescope time for each TRAPPIST-1 planet since each has a different transit duration. For each observed transit (eclipse) we assumed one transit duration worth of out-of-transit (out-of-eclipse) observing time. Considering the following median transit durations for the TRAPPIST-1 planets from Grimm et al. (2018): 36.40 mins for b, 42.37 mins for c, 49.13 mins for d, 57.21 mins for e, 62.60 mins for f, 68.40 mins for g, and 76.7 mins for h, one can calculate expected on-target time per transit/eclipse (before overheads) by multiplying the transit duration by two plus any overheads.

JWST is not always able to point at TRAPPIST-1 due to the star’s proximity to the ecliptic plane. As a result, the star will only be observable to JWST for ~ 100

days per year⁴. Over the course of JWST’s nominal 5 year mission the maximum number of observable transits/eclipses is approximately: 331 for b, 206 for c, 123 for d, 81 for e, 54 for f, 40 for g, and 26 for h. Of course, an extended mission lifetime would allow considerably more observations of the TRAPPIST-1 system.

3.1.3. JWST Emission Spectroscopy

Unlike transmission spectroscopy, which can make use of many JWST instruments that span a broad wavelength range (e.g. NIRCcam, NIRSpec, NIRISS, and MIRI LRS), secondary eclipse spectroscopy of the TRAPPIST-1 planets will only be viable at the longer wavelengths accessible to JWST. This is primarily driven by the increase in eclipse depths with wavelength as the planet-star contrast ratio becomes more favorable.

We find that only MIRI LRS observations of TRAPPIST-1 b and c may potentially rule out a featureless emission spectrum with $\langle \text{SNR} \rangle = 5$ in fewer than 100 observed secondary eclipses. Using an analogous approach to that shown in Figures 13 - 19, MIRI LRS observations of TRAPPIST-1 b may rule out a featureless emission spectrum in 27-47 secondary eclipses if the planet possess a (10 or 92 bar) clear-sky CO₂ atmosphere or a (10 or 100 bar) outgassing O₂ atmosphere, with the 10 bar outgassing O₂ atmosphere the most readily detectable. Over 100 secondary eclipses are required if the planet possesses a desiccated O₂ atmosphere (10 or 100 bars), as these emission spectra appear remarkably featureless between 5-9 μm . For TRAPPIST-1 c we find that MIRI LRS observations could rule out a featureless emission spectrum in 85-100 secondary eclipses if the planet possesses a (10 or 92) bar clear CO₂ atmosphere or a 10 bar O₂ atmosphere with outgassing. Over 100 secondary eclipses are required for all other atmospheric compositions considered for TRAPPIST-1 c, including the CO₂ atmospheres with H₂SO₄ clouds, which have emission spectra similar to the clear CO₂ atmospheres, but with reduced temperature contrasts in the absorbing and emitting spectral regions that effectively mute the features and drive the spectrum towards a featureless blackbody. All of the exterior TRAPPIST-1 planets have emission spectra that will appear indistinguishable from cool blackbodies due to insufficient SNR.

The right panel of Fig. 6 summarizes the best-case-scenario results for detecting the atmospheres of the TRAPPIST-1 planets with JWST emission spectroscopy (red lines) to compare against our filter pho-

⁴ <https://jwst-docs.stsci.edu/display/JTI/JWST+Target+Viewing+Constraints>

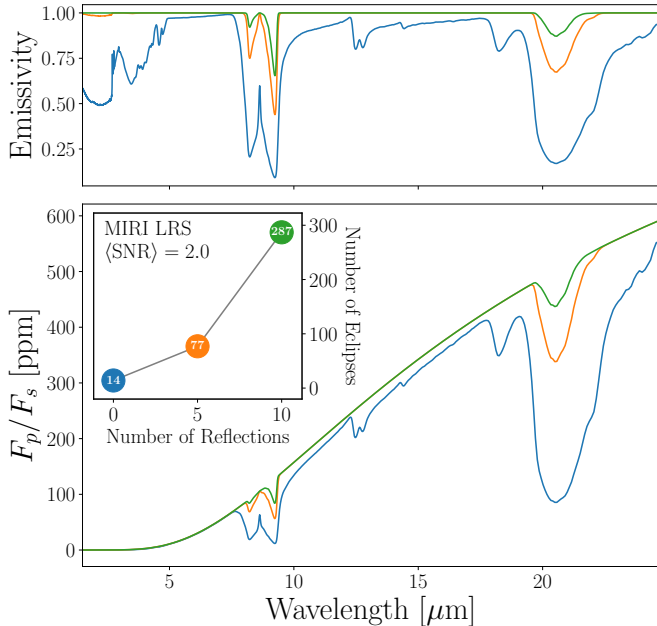


Figure 11. Estimated detectability of pure quartz surface emissivity features in the secondary eclipse spectrum of TRAPPIST-1b with JWST’s MIRI LRS instrument. The top panel shows the MIR effective emissivity of a quartz surface for three different assumed values for the number of surface reflections (see Equation 9): 0 (blue), 5 (orange), and 10 (green). The bottom panel shows theoretical secondary eclipse spectra for TRAPPIST-1b assuming the effective emissivities from the top panel. The inset axis shows the number of secondary eclipses that would be required to observe with MIRI LRS to detect features in the emission spectrum with a $\langle\text{SNR}\rangle = 2.0$, for each of the three assumed effective emissivities. Only an extremely polished pure quartz surface could possibly be detected with JWST.

tometry and transmission spectroscopy results. The number of eclipses required to detect the atmosphere at $\langle\text{SNR}\rangle = 5$ for each of the atmospheric models is shown for observations with MIRI LRS. Compared with transmission spectroscopy, emission spectroscopy is an inefficient method for *detecting* the TRAPPIST-1 planetary atmospheres, particularly for the cooler planets.

If TRAPPIST-1b does not possess an atmosphere, emissivity features from minerals on the surface of the planet are not likely to be detectable in secondary eclipse thermal emission spectra. Figure 11 shows the estimated thermal emission spectrum of TRAPPIST-1b if it is airless and possesses a pure quartz surface. Three different effective emissivities are shown in the top panel, corresponding to 0 (blue), 5 (orange), and 10 (green) surface reflections (see Equation 9). The bottom panel shows the MIR secondary eclipse spectrum for each surface emissivity, assuming the surface is at the (highly optimistic) zero bond albedo equilibrium temperature for

TRAPPIST-1b (392 K). The inset axis shows the number of secondary eclipses that MIRI LRS would have to observe to detect features in each emission spectrum at a weak $\langle\text{SNR}\rangle = 2.0$. Increasing the number of surface reflections results in surface emissivity features that are not detectable.

3.2. Distinguishing Specific Molecules

We now present the sensitivity of each JWST instrument to each gas in the Lincowski et al. (2018) TRAPPIST-1 model transmission spectra. Table 2 lists the molecules for which JWST could weakly detect ($\langle\text{SNR}\rangle = 3.0$) that molecule’s contribution to the spectrum in 100 or fewer transits. For each molecule, the number of transits is listed in parentheses next to each molecular formula along with a footnote identifying which JWST instrument is used for that observation. While in some cases multiple instruments may be sensitive to the same molecule, we list only the instrument that can detect each gas in the minimum number of transits.

The presence of CO_2 dominates the detectability of all the atmospheres simulated in Lincowski et al. (2018) with JWST. Even a relatively small amount of CO_2 (e.g. ~ 290 ppm for the 1 bar H_2O TRAPPIST-1 e) can saturate the strong 2.7, 4.3, 15 μm CO_2 absorption features and lead to the detection of both the atmosphere and CO_2 . As a result, the number of transits necessary to detect spectral features in a transmission spectrum, given in Section 3.1.2, are close to the number of transits necessary to detect CO_2 . In some cases, the number of transits to detect CO_2 is fewer than that needed to simply detect the atmosphere. This is because the spectral model without CO_2 deviates more significantly from the true spectrum than the best-fitting featureless spectrum. In these cases it is important to defer to the number of transits required to rule out a featureless spectrum, because it provides a more realistic fit to the spectrum.

The inner TRAPPIST-1 planets may have several detectable molecules that can be used to distinguish between different evolutionary scenarios. H_2O and SO_2 may be marginally detectable with MIRI LRS transmission spectra of the inner TRAPPIST-1 planets—b, c, and d— if they possess clear sky CO_2 atmospheres. However, if these planets possess H_2SO_4 clouds then the H_2O and SO_2 may be undetectable. Alternatively, if TRAPPIST-1 b, c, and d have oxygen-dominated atmospheres then O_2 should be distinguishable via $\text{O}_2\text{-O}_2$ (O_4) CIA features at 1.06 and 1.27 μm , which are slightly more detectable with NIRSpec G140M/H than the NIRSpec Prism*. An oxygen-dominated planet with outgassing may be distinguished from a completely des-

Table 2. Detectable molecules with transmission spectroscopy for different plausible TRAPPIST-1 planet atmospheres

Planet	Model	Molecules
(Number of transits to $\langle \text{SNR} \rangle = 3.0$)		
T-1b	10 bar CO ₂	CO ₂ (1 ^k), CO(47 ^k), H ₂ O(44 ^f), SO ₂ (40 ^f)
	92 bar CO ₂	CO ₂ (1 ^k), CO(47 ^k), H ₂ O(41 ^f), SO ₂ (38 ^f)
	100 bar O ₂ outgassing	CO ₂ (1 ^k), H ₂ O(2 ^k), O ₃ (11 ^e), O ₂ (3 ^c)
	10 bar O ₂ outgassing	CO ₂ (1 ^k), H ₂ O(1 ^k), O ₂ (4 ^c)
	100 bar O ₂ desiccated	CO ₂ (1 ^k), O ₂ (3 ^c)
T-1c	10 bar O ₂ desiccated	CO(13 ^d), CO ₂ (1 ^k), O ₃ (81 ^f), O ₂ (3 ^c)
	10 bar CO ₂	CO ₂ (1 ^k), H ₂ O(45 ^f), SO ₂ (51 ^f)
	92 bar CO ₂	CO ₂ (1 ^k), H ₂ O(43 ^f), SO ₂ (52 ^f)
	100 bar O ₂ outgassing	CO ₂ (3 ^k), H ₂ O(4 ^k), O ₃ (5 ^e), O ₂ (7 ^c)
	10 bar O ₂ outgassing	CO ₂ (2 ^k), H ₂ O(2 ^k), O ₃ (86 ^f), O ₂ (5 ^c)
	100 bar O ₂ desiccated	CO ₂ (2 ^k), O ₃ (71 ^f), O ₂ (7 ^c)
	10 bar O ₂ desiccated	CO(61 ^k), CO ₂ (1 ^k), O ₃ (64 ^f), O ₂ (6 ^c)
T-1d	10 bar Venus	CO ₂ (3 ^k)
	92 bar Venus	CO ₂ (6 ^k)
T-1d	10 bar CO ₂	CO ₂ (1 ^k), CO(48 ^k), H ₂ O(18 ^f), SO ₂ (27 ^f)
	92 bar CO ₂	CO ₂ (1 ^k), CO(47 ^k), H ₂ O(17 ^f), SO ₂ (27 ^f)
	100 bar O ₂ outgassing	CO ₂ (2 ^k), H ₂ O(2 ^k), O ₃ (2 ^e), O ₂ (3 ^c)
	10 bar O ₂ outgassing	CO ₂ (1 ^k), H ₂ O(2 ^k), O ₃ (32 ^f), O ₂ (3 ^c)
	100 bar O ₂ desiccated	CO ₂ (1 ^k), O ₃ (26 ^f), O ₂ (3 ^c)
	10 bar O ₂ desiccated	CO(49 ^k), CO ₂ (1 ^k), O ₃ (30 ^f), O ₂ (3 ^c)
	10 bar Venus	CO ₂ (6 ^k)
T-1e	92 bar Venus	CO ₂ (7 ^k)
	10 bar CO ₂	CO ₂ (2 ^k), SO ₂ (86 ^f)
T-1e	92 bar CO ₂	CO ₂ (2 ^k), SO ₂ (88 ^f)
	100 bar O ₂ outgassing	CO ₂ (9 ^k), H ₂ O(64 ^k), O ₃ (4 ^k), O ₂ (22 ^c)
	10 bar O ₂ outgassing	CO ₂ (4 ^k), H ₂ O(78 ^k), O ₃ (72 ^e), O ₂ (24 ^c)
	100 bar O ₂ desiccated	CO ₂ (4 ^k), O ₃ (61 ^e), O ₂ (18 ^c)
	10 bar O ₂ desiccated	CO ₂ (3 ^k), O ₃ (40 ^e), O ₂ (19 ^c)
	10 bar Venus	CO ₂ (9 ^k)
	92 bar Venus	CO ₂ (9 ^k)
T-1f	1 bar H ₂ O	CO ₂ (9 ^k), H ₂ O(15 ^k), N ₂ (68 ^e)
	1 bar H ₂ O cloudy	CO ₂ (13 ^k)
T-1f	10 bar CO ₂	CO ₂ (2 ^k), SO ₂ (76 ^f)
	92 bar CO ₂	CO ₂ (2 ^k), SO ₂ (79 ^f)
	100 bar O ₂ outgassing	CO ₂ (7 ^k), O ₃ (2 ^k), O ₂ (23 ^c)
	10 bar O ₂ outgassing	CO ₂ (4 ^k), O ₃ (39 ^e), O ₂ (30 ^c)
	100 bar O ₂ desiccated	CO ₂ (4 ^k), O ₃ (10 ^e), O ₂ (20 ^c)
	10 bar O ₂ desiccated	CO ₂ (3 ^k), O ₃ (7 ^e), O ₂ (20 ^c)
	10 bar Venus	CO ₂ (3 ^k)
T-1g	92 bar Venus	CO ₂ (3 ^k)
	10 bar CO ₂	CO ₂ (2 ^k), SO ₂ (82 ^f)
T-1g	92 bar CO ₂	CO ₂ (2 ^k), SO ₂ (89 ^f)
	100 bar O ₂ outgassing	CO ₂ (9 ^k), O ₃ (2 ^k), O ₂ (36 ^c)
	10 bar O ₂ outgassing	CO ₂ (4 ^k), O ₃ (29 ^e), O ₂ (43 ^c)
	100 bar O ₂ desiccated	CO ₂ (5 ^k), O ₃ (6 ^e), O ₂ (28 ^c)
	10 bar O ₂ desiccated	CO ₂ (3 ^k), O ₃ (5 ^k), O ₂ (28 ^c)
	10 bar Venus	CO ₂ (3 ^k)
	92 bar Venus	CO ₂ (3 ^k)
T-1h	10 bar CO ₂	CO ₂ (2 ^k), SO ₂ (85 ^f)
	92 bar CO ₂	CO ₂ (2 ^k), SO ₂ (86 ^f)
	100 bar O ₂ outgassing	CO ₂ (9 ^k), O ₃ (1 ^k), O ₂ (32 ^c)
	10 bar O ₂ outgassing	CO ₂ (4 ^k), SO ₂ (54 ^f), O ₃ (23 ^e), O ₂ (31 ^c)
	100 bar O ₂ desiccated	CO ₂ (4 ^k), O ₃ (3 ^k), O ₂ (22 ^c)
	10 bar O ₂ desiccated	CO ₂ (3 ^k), O ₃ (4 ^k), O ₂ (22 ^c)
	10 bar Venus	CO ₂ (2 ^k)
92 bar Venus	CO ₂ (2 ^k)	

^c NIRSpec G140H^d NIRSpec G235H^e NIRSpec G395H^f MIRI LRS^k NIRSpec Prism sub512 ngroup6

icated world by detecting H₂O, which is only readily detectable in our models of O₂ planets with outgassing.

TRAPPIST-1 e offers an opportunity to characterize a planet in the habitable zone with JWST. Like the inner TRAPPIST-1 planets, O₂ may be detectable in the spectrum of an oxygen-dominated atmosphere via the O₂-O₂ CIA features. However, modern Earth levels of O₂ and O₃, and Earth geologic levels of CH₄ in a 1 bar N₂-dominated atmosphere are not likely to be detectable. If TRAPPIST-1 e possesses such a habitable environment without clouds, tropospheric H₂O may be detectable using the NIRSpec Prism*. However, with full cloud coverage the detectability of H₂O strongly diminishes and becomes unobservable. The broad 4.3 μm N₂-N₂ CIA feature may be marginally detectable in a 1 bar habitable N₂-dominated atmosphere with NIRSpec G395M/H. The 9.6 μm O₃ feature would require just over 100 transits with MIRI LRS to detect at $\langle \text{SNR} \rangle = 3.0$ in the clear sky 1 bar N₂-dominated atmosphere; approximately twice the number of transits would be required if the planet possesses 100% water cloud coverage.

For the outer planets—TRAPPIST-1 f, g, and h—modest atmospheric characterization with transmission spectroscopy may be possible. In particular, oxygen-dominated atmospheres may be distinguished not only by their prominent O₂-O₂ CIA features, but also by their O₃ features, which become more detectable with the NIRSpec Prism* than the O₂-O₂ features for the coolest TRAPPIST-1 planets.

The observational difficulty with which individual molecules may be detected in a transmission spectrum—bulk atmospheric constituents or trace gases—varies substantially as a function of atmospheric composition. Consequently, the gases that are both relatively easy to detect and unique to a specific atmosphere make optimal testable hypotheses for that atmospheric composition. Figure 12 demonstrates a potential approach for distinguishing between three different atmospheric states for TRAPPIST-1 b using JWST transmission spectroscopy. The models are shown with calculated error bars that correspond to the amount of JWST observing time that would be required to detect specific molecules in the given spectrum.

In the top panel of Fig. 12, the spectrum of a 10 bar desiccated oxygen atmosphere displays prominent O₄ features that may be detected with $\langle \text{SNR} \rangle \sim 5$ in 12 transits with NIRSpec G140H. This is a strong discriminant between an O₂-dominated atmosphere and a CO₂-dominated atmosphere, both of which have strong and detectable CO₂ features.

The spectrum of a 10 bar oxygen atmosphere with outgassing is shown in the middle panel of Fig. 12. This spectrum has similarly detectable O₄ features to the desiccated atmosphere, but also substantial H₂O features (due to Earth levels of geological fluxes) that may be detected with $\langle \text{SNR} \rangle \sim 5$ in just 3 transits with NIRSpec Prism*. Such strong water absorption in an oxygen-dominated atmosphere would indicate incomplete desiccation.

The spectrum of a 10 bar CO₂ atmosphere is shown in the bottom panel of Fig. 12. This spectrum contrasts with the outgassing oxygen atmosphere in the detectability of H₂O. Water in a Venus-like atmosphere is scarce, particularly in the upper atmosphere, which would require ~ 125 transits with either NIRSpec Prism* or MIRI LRS to detect with $\langle \text{SNR} \rangle \sim 5$. The added benefit of making this costly observation with MIRI LRS is that SO₂ could also be detected with $\langle \text{SNR} \rangle \sim 5$ from the 7.3 and 8.7 μm features. Nonetheless, detecting any gases other than CO₂ in a CO₂-dominated atmosphere will be very difficult.

4. DISCUSSION

Our results indicate that JWST observations may be able to place strong constraints on the presence of high mean molecular weight terrestrial atmospheres for all of the TRAPPIST-1 planets and, in some cases, detect individual touchstone molecules that may be used to distinguish between different evolutionary histories that the planets may have undergone.

4.1. Do the TRAPPIST-1 planets have atmospheres?

For detecting the presence of atmospheres on the TRAPPIST-1 planets, we find that NIRSpec Prism observations are optimal. Transmission spectroscopy with the NIRSpec Prism could lead to a $\langle \text{SNR} \rangle = 5$ detection of atmospheric spectral features in as few as 2-11 transits for TRAPPIST-1 b out to TRAPPIST-1 h if the planets lack high altitude aerosols. However, if the TRAPPIST-1 planets possess Venus-like H₂SO₄ aerosols, reaching the same constraints on the presence of atmospheres may require up to 12 times more transits. CO₂ possesses numerous strong absorption bands from the near-through the mid-IR, such as the 2.0, 2.7, 4.2, and 15 μm bands, which significantly contribute to the ability for JWST to detect the terrestrial atmospheres considered in this work.

Our self-consistent Venus-like H₂SO₄ aerosol modeling reveals trends in the detectability of such atmospheres with semi-major axis. Lincowski et al. (2018) found that TRAPPIST-1 b was too hot for Venus-like aerosols to form in the atmosphere, but that H₂SO₄ aerosols could

form in all six exterior planets. These aerosols form at high altitudes in the atmospheres of TRAPPIST-1 c, d, and e and lead to muted CO₂ features that will require about 4-12 times more transits to be detected with JWST. However, TRAPPIST-1 f, g, and h are cool enough for the H₂SO₄ aerosols to form at lower altitudes (Lincowski et al. 2018), and therefore contribute less to their observable transmission spectra such that their atmospheres may be detected in fewer than 2 times the number of transits compared to the clear sky CO₂ cases for the same planets. Cloudy Venus-like atmospheres for TRAPPIST-1 f, g, and h require fewer transits to detect than cloudy Venus-like atmospheres for TRAPPIST-1 c, d, and e.

Secondary eclipse spectroscopy may require a significantly greater JWST time commitment than transmission spectroscopy to achieve comparable constraints on the detection of the TRAPPIST-1 planet atmospheres. Because of its access to longer wavelengths, MIRI LRS is the only JWST instrument capable of observing eclipse spectra of the TRAPPIST-1 planets with high enough SNR to detect absorption features in the spectra that we considered. However, our estimates for the JWST observing time required to detect *emission* spectrum features with MIRI LRS dwarfed the time required for spectral features to be detected in transmission spectra with NIRSpec, NIRISS, and NIRCам (see Figs. 6, 13-19). Furthermore, the disparity between transmission and emission spectroscopy only broadens with semi-major access, making precise MIRI LRS emission spectroscopy beyond TRAPPIST-1c infeasible with JWST. Our self-consistent planet models reveal that atmospheres with high altitude aerosols—that may appear featureless in a transmission spectrum—may also appear featureless in an emission spectrum as thermal flux is emitted and/or scattered from near the top of the cloud deck.

Initial photometric assessments of the TRAPPIST-1 system with MIRI filter photometry are unlikely to provide more efficient preliminary results than transmission spectroscopy in the NIR with NIRSpec, NIRISS, or NIRCам. Our MIRI transit and eclipse photometry modeling showed that detecting the presence of atmospheres would require approximately an order of magnitude more JWST time than NIRSpec Prism transmission spectroscopy. This is due to (1) the higher SNR on transits afforded to NIRSpec near the peak of the stellar SED in the 1-3 μm range, (2) the usefulness of spectral resolution for atmospheric detections via deviations from a featureless spectrum, and (3) the need to observe transits in each MIRI filter separately to gain any meaningful wavelength resolution.

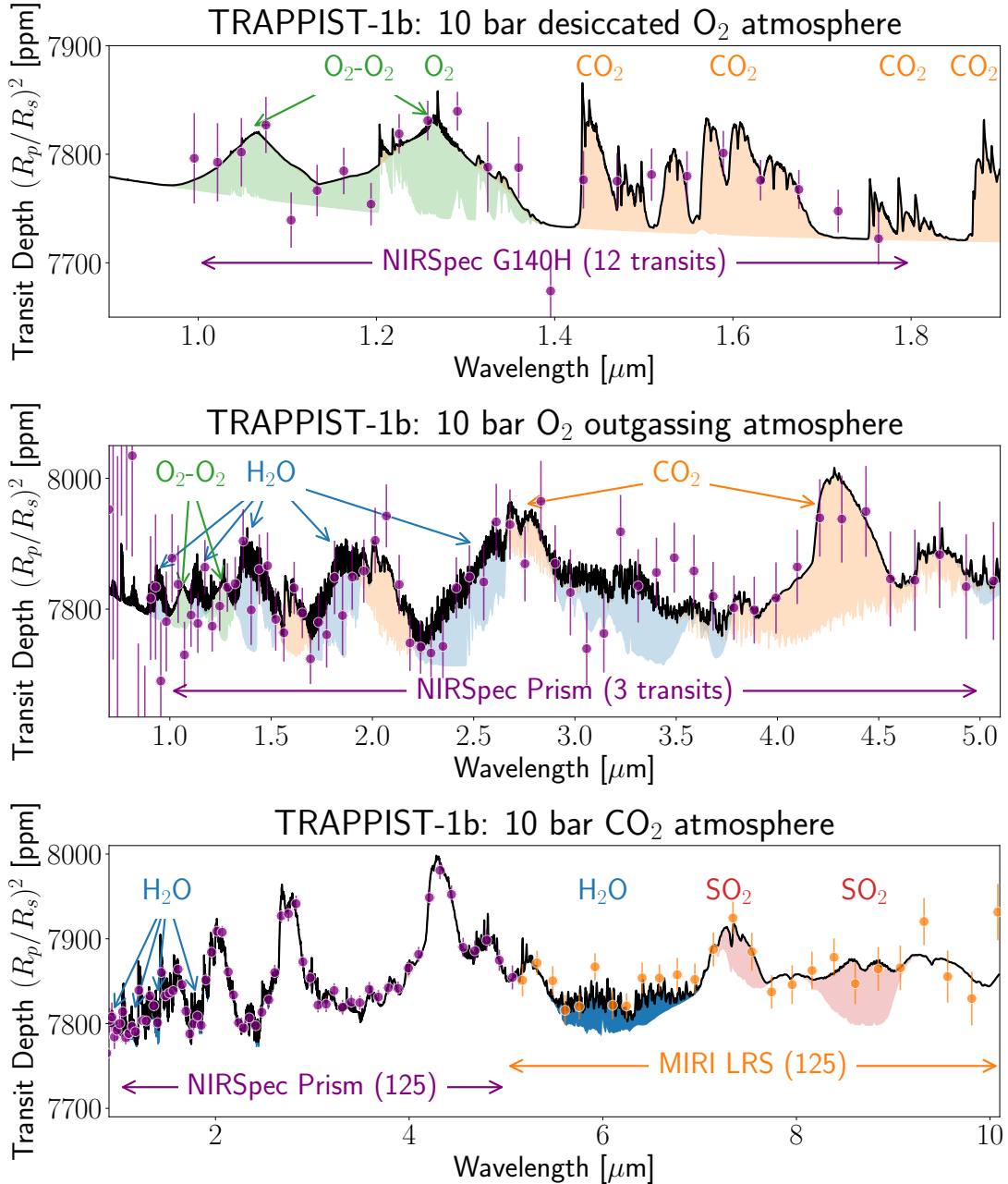


Figure 12. Theoretical transmission spectra of TRAPPIST-1 b assuming three different atmospheric compositions with modeled noise for JWST observations. *Top:* Transmission spectrum of a 10 bar desiccated O₂ atmosphere shown with error bars calculated for 12 transits with NIRSpec G140H—sufficient for $\langle\text{SNR}\rangle \sim 5$ on the O₄ features. *Middle:* Transmission spectrum of a 10 bar outgassing O₂ atmosphere shown with error bars calculated for 3 transits with NIRSpec Prism*—sufficient for $\langle\text{SNR}\rangle \sim 5$ on the H₂O features. *Bottom:* Transmission spectrum of a 10 bar CO₂ atmosphere shown with error bars calculated for 125 transits with NIRSpec Prism*—sufficient for $\langle\text{SNR}\rangle \sim 5$ on the NIR H₂O features—and 125 transits with MIRI LRS—sufficient for $\langle\text{SNR}\rangle \sim 5$ on both the 6 μm H₂O feature and the 7.3 and 8.7 μm SO₂ features.

However, targeted MIRI photometric observations may still provide useful atmospheric constraints. Detecting the presence of atmospheric greenhouse heating may be done by inferring brightness temperatures that exceed the zero bond albedo equilibrium temperature. However, this will depend on the accuracy of MIRI's

absolute flux measurements. Specific wavelength bands where the observed atmosphere is optically thin, and therefore emits from hotter depths, provide the key observable. However, these observations may only be feasible for TRAPPIST-1 b and c due to their higher expected thermal emission. The 11.3 μm MIRI fil-

ter (F1130W) may be optimal for such measurements because it is sufficiently separated from the strongly absorbing $15\ \mu\text{m}$ CO_2 band. The $5.6\ \mu\text{m}$ MIRI filter (F560W) may also be optimal for detecting high thermal emission from TRAPPIST-1 b and c, if saturation on the star can be avoided in this bandpass. Transit and/or eclipse photometry targeting the $15\ \mu\text{m}$ CO_2 band with the F1500W MIRI filter, and neighboring filters, could be used to detect the atmosphere, but our work shows that targeting the strong $4.2\ \mu\text{m}$ CO_2 feature with NIRSpec Prism transmission spectroscopy will be a much more efficient approach for detecting CO_2 in an atmosphere.

Detecting wavelength-dependent surface emissivity features in the emission spectrum of a planet without an atmosphere will be highly unlikely with JWST. Even for the optimistic case—TRAPPIST-1 b with a pure and smooth quartz surface—we find it would require ~ 90 secondary eclipses with MIRI LRS to detect the mid-IR silicate absorption (see Fig. 11). Consequently, detecting surface features on an airless world would be extremely challenging. This validates our assumption that an airless planet will likely appear featureless in emission, and that detecting spectral features due to surface emissivity variations is an inefficient means to confirm that a planet is airless. Furthermore, this strengthens the case for transmission spectroscopy, which can detect the high mean molecular weight atmosphere of a Venus-like planet enshrouded in H_2SO_4 clouds in just ~ 20 -30 transits (for TRAPPIST-1 c, d, and e). However, actually *confirming* that a TRAPPIST-1 planet does not possess an atmosphere—even if featureless spectra lend favor to that hypothesis—will be a very difficult task, that may require thermal phase curve (Selsis et al. 2011; Maurin et al. 2012; Kreidberg & Loeb 2016; Meadows et al. 2018) or planet-planet occultation observations (Luger et al. 2017a) to probe the day-night temperature contrast.

Comparison with Previous Works—Our results are in agreement with previous investigations on optimal ways to detect terrestrial exoplanet atmospheres of different compositions. Although emission spectroscopy has been suggested as a means of detecting terrestrial atmospheres (e.g. Belu et al. 2011), we agree with previous works that transmission spectroscopy is more viable (e.g. Hedelt et al. 2013; Barstow et al. 2016; Barstow & Irwin 2016; Greene et al. 2016), particularly for temperate and cool planets which emit considerably less thermal flux. We agree with B  tr  mieux & Swain (2018) that the JWST integration times needed to detect molecules strongly depend on the composition of the atmosphere—particularly the presence of high altitude aerosols.

Although we considered more atmospheric compositions, our predicted exposure times for the detection of planetary atmospheres agree for the subset of similar atmospheres modeled by Morley et al. (2017), with many of the discrepancies attributable to differences in the assumed planetary masses used in the transmission spectrum models. Our work and that of Morley et al. (2017) has a common focus of distinguishing clear sky Venus-like atmospheres from a featureless spectrum with the NIRSpec/G235 instrument, which offers a basis for comparison. The detectability of these atmospheres is dominated by CO_2 features, which are largely unaffected by photochemistry, which was not included in Morley et al. (2017). We find that a 10 bar CO_2 atmosphere would require 5, 8, 4, 17, 15, 16, and 15 transits to distinguish TRAPPIST-1 b, c, d, e, f, g, and h, respectively, from a featureless spectrum, and Morley et al. (2017) find that a 1 bar aerosol-free Venus-like atmosphere would require 6, 36, 13, 4, 17, 10, and 4 transits.

The cases of largest disagreement (e.g. c, e, h) appear consistent with the different masses used in each study. Planet mass affects the atmospheric scale height (via the surface gravity) and therefore the size and detectability of molecular features in a transmission spectrum. Morley et al. (2017) used masses from Wang et al. (2017), with the exception of TRAPPIST-1 f, for which the mass from Gillon et al. (2017) was used. In this paper, and in Lincowski et al. (2018), we use the TRAPPIST-1 planet masses from Grimm et al. (2018). For the case of TRAPPIST-1 c where we use a significantly smaller planet mass than Morley et al. (2017) we find that fewer transits are required to detect spectral features in transit. For the cases of TRAPPIST-1 e and h where we use a significantly larger planet mass than Morley et al. (2017) we find that more transits are required to detect spectral features. This scaling with mass is consistent with the findings of Morley et al. (2017) when they repeated calculations with masses derived from the Weiss & Marcy (2014) mass-radius relationship, and further underscores the need for accurate masses for spectral modeling and fitting.

Our focus on thicker atmospheres (1-100 bar) than Morley et al. (2017) (0.01-1 bar) both explains discrepancies between the studies and further demonstrates that such thick and aerosol-free atmospheres may be more easily detected than thinner atmospheres. Our results for TRAPPIST-1 d, where our masses agree best, show 9 fewer transits required to detect spectral features than Morley et al. (2017), which is consistent with different planet surface pressures used in each study. Morley et al. (2017) demonstrated a trend of increasing atmospheric detectability with increasing surface pres-

sure in simulations of 0.01, 0.1, and 1 bar CO₂ atmospheres. Our results continue this nearly linear trend in log-pressure out to 10 bars. However, our 92 bar CO₂ atmospheres are consistent with the detectability of our 10 bar atmospheres, indicating that this trend in pressure saturates for thick atmospheres as the planet surface drops below the atmospheric regions that are sensed with transmission spectroscopy.

The Krissansen-Totton et al. (2018) work on the detectability of biogenic gases in an anoxic atmosphere for TRAPPIST-1 e with JWST suggests that relatively few transits are required to constrain atmospheric abundances. Krissansen-Totton et al. (2018) showed that a retrieval using ~ 10 transits of TRAPPIST-1 e with the NIRSpec Prism was sufficient to begin to constrain the abundances of CO, CO₂, and CH₄. Consequently, the 13 transits of TRAPPIST-1 e that we show may be required to detect a clear 1 bar H₂O atmosphere to a $\langle \text{SNR} \rangle = 5$, may also provide spectra that are sufficient to begin to constrain molecular abundances in an atmospheric retrieval framework.

HST transmission spectroscopy of hot gaseous exoplanets has demonstrated how the presence of clouds and hazes can diminish sensitivity to molecular absorption features (e.g. Berta et al. 2012; Ehrenreich et al. 2014; Knutson et al. 2014; Kreidberg et al. 2014; Nikolov et al. 2015; Sing et al. 2016), but we know *a priori* that planets with such large radii must have atmospheres. However, for terrestrials we will rely on absorption features to test for the presence of atmospheres, and clouds and hazes, if present, will make this more difficult. Batalha et al. (2018) concluded that 10 transits should be sufficient to detect the dominant molecular absorber in the transmission spectrum of TRAPPIST-1f when observed using a partial saturation strategy with the NIRSpec Prism, and that additional observations are unlikely to reveal more information. While our results agree with Batalha et al. (2018) for the case of clear atmospheres, cloudy and/or hazy terrestrial atmospheres may require significantly more observations. Venus-like planets with H₂SO₄ aerosols tend to require more than 10 transits (and up to ~ 30 for TRAPPIST-1e) to reach the same confidence in the detection of the atmosphere. We recommend testing the hypothesis that a TRAPPIST-1 (or similar) planet has a *clear* atmosphere in ≤ 10 transits, and then evaluating the scientific value of additional transits to test the hypothesis that the planet has aerosols.

4.2. *What is the nature of the TRAPPIST-1 planet atmospheres?*

Detecting specific molecules in JWST transmission spectra of the TRAPPIST-1 planets may be possible, and allow for the discrimination between different climate/composition states and evolutionary histories. As previously stated, CO₂ should be the easiest molecule for JWST to detect in the atmospheres of the TRAPPIST-1 planets. Due to its prevalence in these simulated atmospheres *regardless of evolutionary history*, CO₂ makes for a strong indicator of a terrestrial atmosphere, but a weak discriminant of specific atmospheric state. Furthermore, CO₂ produces nearly the same strength features regardless of atmospheric abundance, particularly the 4.3 and 15 μm bands, which are saturated in a Venus-like atmosphere, an O₂ outgassing atmosphere, and an Earth-like atmosphere, even though the abundance ranges from 90 bars down to 360 ppm (Lincowski et al. 2018). Other molecules, such as O₂, O₃, H₂O, and SO₂, may be detectable with JWST and may help to distinguish between the suite of atmospheres that we considered.

Although oxygen as a biosignature may not be detectable for the potentially habitable TRAPPIST-1 planets, oxygen as a remnant of pre-main-sequence water loss may be easily detected or ruled out. We find that biogenic O₂ in the atmosphere of TRAPPIST-1e may be too difficult to detect with JWST, but the 9.6 μm O₃ feature may be weakly detectable at $\langle \text{SNR} \rangle = 3$ in over 100 transits with MIRI LRS, which is in general agreement with the findings of Wunderlich et al. (2019). However, the 1.06 and 1.27 μm O₂-O₂ CIA features are key discriminants of a planet that has an oxygen abundance greatly exceeding biogenic oxygen production on Earth and may therefore indicate a planet that has undergone vigorous water photolysis and subsequent loss during the protracted super-luminous pre-main-sequence phase faced by late M dwarfs (Luger & Barnes 2015; Schwieterman et al. 2016). We find that NIRSpec G140M/H is the optimal JWST instrument for detecting these O₂-O₂ features and could lead to their detection in as few as 7-9, 15, 8, 49-67, 55-82, 79-100, and 62-89 transits of TRAPPIST-1b, c, d, e, f, g, and h, respectively, should they possess such an atmosphere. These quoted number of transits may be sufficient to rule out the existence of oxygen-dominated atmospheres in the TRAPPIST-1 system. Additional evidence of ocean loss could be provided by detection of isotope fractionation, which may also be possible in as few as 11 transits with JWST, for strong isotopologue bands such as HDO (Lincowski et al. 2019).

Detecting ozone absorption may be another strong indicator of a post-runaway, oxygen-dominated atmosphere. For the 10 bar desiccated O₂ atmospheres,

ozone absorption features become more detectable for the outer planets. Targeting O_3 at $9.6 \mu\text{m}$ with MIRI LRS is optimal for the inner planets (b, c, d, e), although it may require upwards of 100 transits to detect at $\langle\text{SNR}\rangle = 5$. However, targeting the weaker O_3 bands between $3 - 5 \mu\text{m}$ with NIRSpec G395M/H or NIRSpec Prism is optimal for the outer planets (f, g, h), due to their larger ozone column abundances. The O_2 - O_2 CIA bands for these cooler, desiccated planets are more difficult to detect, which may make O_3 a more efficient observational discriminant for such a planet.

The photochemistry underlying the detectable ozone buildup in the cooler planets has implications beyond the TRAPPIST-1 system. Lincowski et al. (2018) noted that the competing effects of the Chapman cycle (with declining photolysis rates with distance from the star), was primarily responsible for the ozone accumulation in the atmospheres of the outer planets, an effect previously noticed by Grenfell et al. (2007). While this is a driving factor, the differences among the planets can more specifically be attributed to catalytic cycles of nitrogen oxides (primarily, N_2O , NO , and NO_2), which drive the destruction of O_3 , as in the stratosphere of Earth (Seinfeld & Pandis 2006). Because these atmospheres contain N_2 , O^1D produced from photolysis of oxygen-bearing molecules can react with N_2 to generate nitrogen oxides. The availability of O^1D declines with distance from the star due to lower UV fluxes. Beginning with planet e, the production of nitrogen oxides declines substantially, removing them as a mechanism for the destruction of O_3 , so that O_3 accumulates and becomes well-mixed, generating a large column density. In the atmosphere of an O_2 -dominated atmosphere without N_2 , O_3 levels would likely be higher due to the lack of the nitrogen oxide catalysts.

Detecting water in the atmospheres of the TRAPPIST-1 planets may also help to constrain evolutionary scenarios. The presence of water may be readily detectable for TRAPPIST-1 b, c, and d with the NIRSpec Prism* if they possess high O_2 atmospheres that have not been completely desiccated. High O_2 atmospheres for planets that exited the pre-main-sequence with their atmospheres and interiors completely desiccated, however, will have no water to detect, making water in an oxygen-dominated atmosphere a potentially detectable discriminant of incomplete desiccation or outgassing from the interior. In CO_2 -dominated atmospheres, H_2O may be prohibitively difficult to detect due to its scarcity in the atmospheres of Venus-like worlds, before even considering obscuration by H_2SO_4 clouds.

Detecting water in the atmosphere of one of the potentially habitable TRAPPIST-1 planets could indirectly

hint at surface habitability (Robinson 2018), but this will be challenging for JWST, even with an ideal system like TRAPPIST-1. Tropospheric H_2O may be detectable in the transmission spectrum of TRAPPIST-1 e in ~ 35 transits with NIRSpec Prism* should the planet have a clear-sky 1-bar N_2/O_2 atmosphere with H_2O . However, the cold trap that keeps water vapor concentrated in the lower atmosphere makes habitability difficult to infer with transmission spectroscopy, which cannot readily probe surface environments. Additionally, we find that 100% cloud coverage strongly increases the required JWST time to detect H_2O in such a habitable atmosphere. Given these difficulties for detecting water in the atmosphere of a HZ planet with JWST, robust habitability assessments may ultimately require a future direct imaging telescope that can readily probe rocky planet surfaces to search for more direct evidence of surface liquid water (e.g. Cowan et al. 2009; Robinson et al. 2010; Lustig-Yaeger et al. 2018).

4.3. Further Considerations

The results in this paper lean optimistic, and therefore represent lower limits on the amount of observing time needed to detect and characterize evolved terrestrial atmospheres in the TRAPPIST-1 system. As a result, TRAPPIST-1 observing plans that include fewer transits/eclipses than reported here may require additional observations to make robust inferences on the existence and nature of atmospheres. One source of optimism is that our $\langle\text{SNR}\rangle$ approach (see Equation 6) to atmospheric and molecular detection, rather than a full atmospheric retrieval, implicitly assumes that any retrieval will have converged on the true underlying spectrum. As a result, our signal-to-noise metric is not equal to a detection of that specific atmosphere to a given significance (e.g. 3σ). In practice, many different atmospheric compositions will likely be capable of fitting JWST spectra of TRAPPIST-1 planets, potentially leaving large regions of atmospheric parameter space unconstrained. Thus, the confidence of any “one” composition representing the true state of the planet may remain low despite having high confidence in the presence of features in the spectrum that would indicate the presence an atmosphere. Our approach is simply a wavelength range and resolution agnostic method to quantify the detectability of spectral signals emanating from self-consistent atmospheres above the expected noise of JWST.

Our calculations also lean optimistic because we have neglected astrophysical and systematic sources of noise that may make precise time-series exoplanet observations with JWST more difficult than our estimates sug-

gest. Stellar effects such as limb-darkening (e.g. Csizmadia et al. 2013) and heterogeneous photospheres (e.g. Rackham et al. 2016; Rackham et al. 2018; Zhang et al. 2018) are major concerns for precision exoplanet transmission spectroscopy. These effects may be particularly perilous for observations of planets orbiting low mass stars, as the stars may contain large, cool spots and absorbing molecules in their photospheres. We also did not assume a systematic noise floor for any JWST instruments (e.g. Greene et al. 2016), but this is likely optimistic in terms of the currently unknown on-target performance. Astrophysical and systematic effects must be well understood to detect molecular features at the ~ 10 ppm level, where many terrestrial features reside. However, many of the major absorption features in our TRAPPIST-1 planet spectral models are much larger and more detectable, spanning 50-200 ppm.

During the preparation of this paper, a new version of *Pandora* was released (version 1.3) that increased JWST background noise predictions by 10-40 ppm. For bright targets like TRAPPIST-1 where the noise budget is dominated by stellar photon noise, such an increase in the background has a negligible effect on our estimated number of transits and eclipses to detect and characterize exoplanet atmospheres in the near- through the mid-IR.

We considered a limited number of atmospheres that may not resemble the true state of the TRAPPIST-1 planets, especially since the star’s UV spectrum is poorly constrained. Here, as in Lincowski et al. (2018), we used a UV spectrum scaled from measurements of the nearby mid M dwarf Proxima Centauri, but these stars have slightly different spectral types and activity levels. Recently, three synthetic SEDs have been produced by Peacock et al. (2019) for TRAPPIST-1, which are constrained by the Lyman alpha flux and upper limits of GALEX UV photometry. These synthetic spectra differ by having higher NUV and a different distribution of FUV flux than Lincowski et al. (2018), which could slightly change the photochemistry of these planetary atmospheres and the observable molecular absorption in their upper atmospheres. However, only observations—including those outlined in this paper—will ultimately reveal what planetary processes dominate in sculpting the observable atmospheric signatures of terrestrial exoplanets, particularly those orbiting M dwarfs. In the mean time, further study is warranted on the range of possible atmospheric conditions for the TRAPPIST-1 planets, particularly photochemically and climatically self-consistent reducing atmospheres (e.g. Arney et al. 2017), and UV characterizations of late M dwarfs to im-

prove photochemical predictions and interpretation of observations.

Although the atmospheric states considered in this paper represent only a selection of possible states, many of their characteristics and molecular features may exist in other atmospheres, making our results apply more broadly. For example, the strength of the H₂O, CO₂, and O₃ bands in the O₂-dominated outgassing atmospheres may be similar in other clear atmospheres that may contain more inert gasses, like N₂. Our JWST detectability calculations for these gases may be useful beyond that particular atmospheric case. The O₂-O₂ features, however, are specific evidence of high O₂ content. Since all of the atmospheres considered in this work were high mean molecular weight, our results help to elucidate the detectability of such atmospheres and the molecules within, even if the true compositions differ.

Constraining the atmospheres of Earth-size planets transiting even the smallest stars like TRAPPIST-1 will require pushing the limits of JWST. As we demonstrated with the NIRSpec Prism partial saturation, alternate JWST modes that can improve observations of transiting exoplanets can enhance the science return, and dramatically decrease the time investment required to detect and characterize terrestrial atmospheres. Although modes such as NIRCams’ Dispersed Hartmann Sensor (DHS; Schlawin et al. 2017) and high efficiency readout patterns for NIRSpec Prism (Batalha et al. 2018) have not been officially approved, they represent promising avenues towards improved JWST observations that may ultimately make the difference in enabling JWST to constrain terrestrial exoplanet atmospheric compositions.

5. CONCLUSION

We investigated the potential to detect and characterize the atmospheres of all seven known TRAPPIST-1 exoplanets with JWST. Although the planets are small and likely possess high mean molecular weight atmospheres with relatively low scale heights, we found that many molecular absorption features may be detectable with JWST in ~ 2 -15 transits. These observations may be used to diagnose the presence of atmospheres and, in some cases, discriminate between different plausible atmospheric compositions.

However, we find that an initial photometric assessment of the TRAPPIST-1 planets with MIRI is, perhaps non-intuitively, not as efficient as spectroscopic atmosphere detection in the NIR. To achieve comparable constraints on the detection of atmospheres approximately an order of magnitude more transits or eclipses

will need to be observed with MIRI, compared to transits observed with spectrometers in the NIR.

Transmission spectroscopy with NIRSpec Prism may be the most efficient path to detect the presence of atmospheres for the TRAPPIST-1 planets, via detecting CO₂ bands between 1-5 μm . Venus-like atmospheres with high altitude H₂SO₄ aerosols will be more difficult to detect in transmission and emission spectra, however, these aerosols will form at lower altitudes for the temperate and cooler planets such that they obscure less molecular absorption in transmission spectra. Furthermore, post-runaway oxygen-dominated worlds may be identified in transmission using (1) O₂-O₂ CIA observed with NIRSpec G140M/H, NIRSpec Prism, or NIRISS SOSS, or (2) O₃ absorption observed with MIRI LRS (for b, c, d, and e) or NIRSpec G395M/H (for f, g, and h). If TRAPPIST-1 e is habitable and cloud-free, water could be detected in the troposphere with NIRSpec Prism in about 35 transits, but the presence of water clouds could completely obscure the water vapor absorption features.

We outlined a particular path for characterising the TRAPPIST-1 planets with JWST that narrows down the possible evolutionary histories that the planets may have trod to exist in their current observable states. We recommend using transmission spectroscopy to

1. detect the planet atmospheres via CO₂ absorption;
2. detect or rule out a post-runaway oxygen-dominated atmospheres via O₂-O₂ CIA or O₃ absorption;

3. constrain the extent of (atmosphere and interior) desiccation, and potentially the habitability, via the H₂O abundance.

However, our results may be used to construct countless additional observing strategies that best augment existing projects and proposals with our testable hypotheses on the nature of TRAPPIST-1 system of Earth-sized exoplanets.

We thank Eric Agol for insights into our photometric signal-to-noise calculations, Joshua Bandfield and Elena Amador for crucial discussions on the emissivity signatures of rocks, and Rodrigo Luger for countless useful discussions that contributed to this work. We also thank the anonymous referee whose helpful comments contributed to the quality and clarity of this paper. This work was supported by NASA's Virtual Planetary Laboratory under NASA Astrobiology Institute Cooperative Agreement Number NNA13AA93A, and Grant Number 80NSSC18K0829. This work benefited from participation in the NASA Nexus for Exoplanet Systems Science research coordination network. This work made use of the advanced computational, storage, and networking infrastructure provided by the Hyak supercomputer system at the University of Washington.

Software: Astropy (Astropy Collaboration et al. 2013; Price-Whelan et al. 2018), Matplotlib (Hunter 2007), Numpy (van der Walt et al. 2011), SMART (Meadows & Crisp 1996), Pandeia (Pontoppidan et al. 2016), PandExo (Batalha et al. 2017; Batalha et al. 2018), pysynphot (STScI Development Team 2013)

REFERENCES

- Airapetian, V. S., Gloer, A., Khazanov, G. V., et al. 2017, *ApJL*, 836, L3
- Anglada-Escudé, G., Amado, P. J., Barnes, J., et al. 2016, *Nature*, 536, 437
- Arney, G., Domagal-Goldman, S. D., & Meadows, V. S. 2018, *Astrobiology*, 18, 311
- Arney, G. N., Meadows, V. S., Domagal-Goldman, S. D., et al. 2017, *ApJ*, 836, 49
- Astropy Collaboration, Robitaille, T. P., Tollerud, E. J., et al. 2013, *A&A*, 558, A33
- Bagnasco, G., Kolm, M., Ferruit, P., et al. 2007, in *Proc. SPIE*, Vol. 6692, *Cryogenic Optical Systems and Instruments XII*, 66920M
- Baraffe, I., Homeier, D., Allard, F., & Chabrier, G. 2015, *A&A*, 577, A42
- Barstow, J. K., Aigrain, S., Irwin, P. G. J., Kendrew, S., & Fletcher, L. N. 2016, *Monthly Notices of the Royal Astronomical Society*, 458, 2657
- Barstow, J. K., & Irwin, P. G. J. 2016, *Monthly Notices of the Royal Astronomical Society*, 461, L92
- Batalha, N., Stevenson, K., Hill, M., et al. 2018, *natashabatalha/PandExo: Starting PandExo Releases*, doi:10.5281/zenodo.1256955
- Batalha, N. E., Lewis, N. K., Line, M. R., Valenti, J., & Stevenson, K. 2018, *ApJL*, 856, L34
- Batalha, N. E., Mandell, A., Pontoppidan, K., et al. 2017, *Publications of the Astronomical Society of the Pacific*, 129, 064501
- Belu, A. R., Selsis, F., Morales, J.-C., et al. 2011, *Astronomy & Astrophysics*, 525, A83

- Berta, Z. K., Charbonneau, D., Désert, J.-M., et al. 2012, *The Astrophysical Journal*, 747, 35
- Berta-Thompson, Z. K., Irwin, J., Charbonneau, D., et al. 2015, *Nature*, 527, 204
- Bétrémieux, Y., & Kaltenegger, L. 2014, *The Astrophysical Journal*, 791, 7
- Bétrémieux, Y., & Swain, M. R. 2018, ArXiv e-prints, arXiv:1801.00738
- Bolmont, E., Selsis, F., Owen, J. E., et al. 2017, *MNRAS*, 464, 3728
- Bouchet, P., García-Marín, M., Lagage, P.-O., et al. 2015, *PASP*, 127, 612
- Cowan, N. B., Agol, E., Meadows, V. S., et al. 2009, *ApJ*, 700, 915
- Cowan, N. B., Greene, T., Angerhausen, D., et al. 2015, *PASP*, 127, 311
- Csizmadia, S., Pasternacki, T., Dreyer, C., et al. 2013, *A&A*, 549, A9
- de Wit, J., Wakeford, H. R., Gillon, M., et al. 2016, *Nature*, 537, 69
- de Wit, J., Wakeford, H. R., Lewis, N. K., et al. 2018, *Nature Astronomy*, 2, 214
- Delrez, L., Gillon, M., Triaud, A. H. M. J., et al. 2018, *MNRAS*, 475, 3577
- Dittmann, J. A., Irwin, J. M., Charbonneau, D., et al. 2017, *Nature*, 544, 333
- Dong, C., Jin, M., Lingam, M., et al. 2018, *Proceedings of the National Academy of Science*, 115, 260
- Doyon, R., Hutchings, J. B., Beaulieu, M., et al. 2012, in *Proc. SPIE*, Vol. 8442, *Space Telescopes and Instrumentation 2012: Optical, Infrared, and Millimeter Wave*, 84422R
- Ehrenreich, D., Bonfils, X., Lovis, C., et al. 2014, *Astronomy & Astrophysics*, 570, A89
- Feng, Y. K., Robinson, T. D., Fortney, J. J., et al. 2018, *AJ*, 155, 200
- Ferruit, P., Birkmann, S., Böker, T., et al. 2014, in *Proc. SPIE*, Vol. 9143, *Space Telescopes and Instrumentation 2014: Optical, Infrared, and Millimeter Wave*, 91430A
- García-Sage, K., Glöcker, A., Drake, J. J., Gronoff, G., & Cohen, O. 2017, *ApJL*, 844, L13
- Gillon, M., Jehin, E., Lederer, S. M., et al. 2016, *Nature*, 533, 221
- Gillon, M., Triaud, A. H. M. J., Demory, B.-O., et al. 2017, *Nature*, 542, 456
- Glasse, A., Rieke, G. H., Bauwens, E., et al. 2015, *PASP*, 127, 686
- Greene, T., Beichman, C., Eisenstein, D., et al. 2007, in *Proc. SPIE*, Vol. 6693, *Techniques and Instrumentation for Detection of Exoplanets III*, 66930G
- Greene, T. P., Line, M. R., Montero, C., et al. 2016, *The Astrophysical Journal*, 817, 17
- Greene, T. P., Kelly, D. M., Stansberry, J., et al. 2017, *Journal of Astronomical Telescopes, Instruments, and Systems*, 3, 035001
- Grenfell, J. L., Grießmeier, J.-M., Patzer, B., et al. 2007, *Astrobiology*, 7, 208
- Grimm, S. L., Demory, B.-O., Gillon, M., et al. 2018, *A&A*, 613, A68
- Hedelt, P., von Paris, P., Godolt, M., et al. 2013, *Astronomy & Astrophysics*, 553, A9
- Hu, R., Ehlmann, B. L., & Seager, S. 2012, *ApJ*, 752, 7
- Hunter, J. D. 2007, *Computing In Science & Engineering*, 9, 90
- Husser, T. O., Wende-von Berg, S., Dreizler, S., et al. 2013, *A&A*, 553, A6
- Kalirai, J. 2018, *Contemporary Physics*, 59, 251
- Kendrew, S., Scheithauer, S., Bouchet, P., et al. 2015, *PASP*, 127, 623
- Kirkland, L. E., Herr, K. C., & Adams, P. M. 2003, *Journal of Geophysical Research (Planets)*, 108, 5137
- Knutson, H. A., Benneke, B., Deming, D., & Homeier, D. 2014, *Nature*, 505, 66
- Kreidberg, L., & Loeb, A. 2016, *ApJL*, 832, L12
- Kreidberg, L., Bean, J. L., Désert, J.-M., et al. 2014, *Nature*, 505, 69
- Krissansen-Totton, J., Garland, R., Irwin, P., & Catling, D. C. 2018, *AJ*, 156, 114
- Liebert, J., & Gizis, J. E. 2006, *PASP*, 118, 659
- Lincowski, A., Lustig-Yaeger, J., & Meadows, V. 2019, in *American Astronomical Society Meeting Abstracts*, Vol. 233, *American Astronomical Society Meeting Abstracts* 233, 226.05
- Lincowski, A. P., Meadows, V. S., Crisp, D., et al. 2018, *ApJ*, 867, 76
- Luger, R., & Barnes, R. 2015, *Astrobiology*, 15, 119
- Luger, R., Barnes, R., Lopez, E., et al. 2015, *Astrobiology*, 15, 57
- Luger, R., Lustig-Yaeger, J., & Agol, E. 2017a, *ApJ*, 851, 94
- Luger, R., Sestovic, M., Kruse, E., et al. 2017b, *Nature Astronomy*, 1, 0129
- Lustig-Yaeger, J., Meadows, V. S., Tovar Mendoza, G., et al. 2018, *AJ*, 156, 301
- Maurin, A. S., Selsis, F., Hersant, F., & Belu, A. 2012, *A&A*, 538, A95
- Meadows, V. S., & Crisp, D. 1996, *J. Geophys. Res.*, 101, 4595

- Meadows, V. S., Arney, G. N., Schwieterman, E. W., et al. 2018, *Astrobiology*, 18, 133
- Miller-Ricci, E., Seager, S., & Sasselov, D. 2009, *The Astrophysical Journal*, 690, 1056
- Misra, A., Meadows, V., & Crisp, D. 2014, *The Astrophysical Journal*, 792, 61
- Moran, S. E., Hörst, S. M., Batalha, N. E., Lewis, N. K., & Wakeford, H. R. 2018, ArXiv e-prints, arXiv:1810.05210
- Morley, C. V., Kreidberg, L., Rustamkulov, Z., Robinson, T., & Fortney, J. J. 2017, *ApJ*, 850, 121
- Morris, B. M., Agol, E., Davenport, J. R. A., & Hawley, S. L. 2018, *ApJ*, 857, 39
- Nicodemus, F. E. 1965, *ApOpt*, 4, 767
- Nikolov, N., Sing, D. K., Burrows, A. S., et al. 2015, *Monthly Notices of the Royal Astronomical Society*, 447, 463
- Peacock, S., Barman, T., Shkolnik, E. L., Hauschildt, P. H., & Baron, E. 2019, *ApJ*, 871, 235
- Pontoppidan, K. M., Pickering, T. E., Laidler, V. G., et al. 2016, in *Proc. SPIE*, Vol. 9910, *Observatory Operations: Strategies, Processes, and Systems VI*, 991016
- Price-Whelan, A. M., Sipőcz, B. M., Günther, H. M., et al. 2018, *AJ*, 156, 123
- Rackham, B., Espinoza, N., Apai, D., et al. 2016, arXiv preprint arXiv:1612.00228
- Rackham, B. V., Apai, D., & Giampapa, M. S. 2018, *ApJ*, 853, 122
- Robinson, T. D. 2017, *ApJ*, 836, 236
- . 2018, *Characterizing Exoplanet Habitability*, 67
- Robinson, T. D., & Crisp, D. 2018, *JQSRT*, 211, 78
- Robinson, T. D., Meadows, V. S., & Crisp, D. 2010, *ApJL*, 721, L67
- Roettenbacher, R. M., & Kane, S. R. 2017, *ApJ*, 851, 77
- Rugheimer, S., Kaltenegger, L., Segura, A., Linsky, J., & Mohanty, S. 2015, *ApJ*, 809, 57
- Schaefer, L., Wordsworth, R. D., Berta-Thompson, Z., & Sasselov, D. 2016, *ApJ*, 829, 63
- Schlawin, E., Rieke, M., Leisenring, J., et al. 2017, *PASP*, 129, 015001
- Schwieterman, E. W., Meadows, V. S., Domagal-Goldman, S. D., et al. 2016, *The Astrophysical Journal Letters*, 819, L13
- Schwieterman, E. W., Kiang, N. Y., Parenteau, M. N., et al. 2018, *Astrobiology*, 18, 663
- Segura, A., Kasting, J. F., Meadows, V., et al. 2005, *Astrobiology*, 5, 706
- Seinfeld, J., & Pandis, S. 2006, *Atmospheric Chemistry and Physics*
- Selsis, F., Wordsworth, R. D., & Forget, F. 2011, *A&A*, 532, A1
- Sing, D. K., Fortney, J. J., Nikolov, N., et al. 2016, *Nature*, 529, 59
- STScI Development Team. 2013, *pysynphot: Synthetic photometry software package*, *Astrophysics Source Code Library*, ascl:1303.023
- van der Walt, S., Colbert, S. C., & Varoquaux, G. 2011, *Computing in Science and Engineering*, 13, 22
- Van Grootel, V., Fernandes, C. S., Gillon, M., et al. 2018, *ApJ*, 853, 30
- Vida, K., Kővári, Z., Pál, A., Oláh, K., & Kriskovics, L. 2017, *ApJ*, 841, 124
- Wang, S., Wu, D.-H., Barclay, T., & Laughlin, G. P. 2017, ArXiv e-prints, arXiv:1704.04290
- Weiss, L. M., & Marcy, G. W. 2014, *ApJL*, 783, L6
- Wordsworth, R. D., Schaefer, L. K., & Fischer, R. A. 2018, *AJ*, 155, 195
- Wunderlich, F., Godolt, M., Grenfell, J. L., et al. 2019
- Zhang, Z., Zhou, Y., Rackham, B. V., & Apai, D. 2018, *AJ*, 156, 178

APPENDIX

A. SIGNAL-TO-NOISE RATIO ON TRANSIT AND ECLIPSE DEPTHS

Transit and eclipse depth measurements are both relative to the out-of-occultation measurement, and thus require accounting for photon fluence in- and out-of-the the event of interest. Below we derive the signal-to-noise on measurements of transit and eclipse depths by considering the signal as the occultation depth, which must be calculated from the difference between in- and out-of-event observations, and the noise by propagating individual measurement errors through the signal calculation.

For primary transit, the signal of interest is the number of photons missing when the star is occulted by the planet. Neglecting photons emitted and reflected by the planet prior to and during transit, the out-of-transit photon fluence is measured as

$$N_{\text{out}} = (N_s + N_{bg})n_{\text{out}}, \quad (\text{A1})$$

where n_{out} is the time of measurement outside of transit in units of the transit duration, and N_s and N_{bg} are the total number of photons counted over a transit duration. The in-transit photon fluence measured is

$$N_{tr} = N_s \left(1 - \left(\frac{R_p}{R_s} \right)^2 \right) + N_{bg}. \quad (\text{A2})$$

The number of stellar photons blocked by the planet can be estimated from

$$N_{sp} = N_{\text{out}}/n_{\text{out}} - N_{tr}, \quad (\text{A3})$$

this is the signal we seek to measure. The noise on N_{sp} can be calculated by considering the variance given standard uncorrelated error propagation:

$$\sigma^2 = \left(\frac{\partial N_{sp}}{\partial N_{\text{out}}} \right)^2 \sigma N_{\text{out}}^2 + \left(\frac{\partial N_{sp}}{\partial N_{tr}} \right)^2 \sigma N_{tr}^2 \quad (\text{A4})$$

$$= \left(\frac{1}{n_{\text{out}}} \right)^2 N_{\text{out}} + (-1)^2 N_{tr} \quad (\text{A5})$$

$$= \frac{(N_s + N_{bg})}{n_{\text{out}}} + N_s \left(1 - \left(\frac{R_p}{R_s} \right)^2 \right) + N_{bg} \quad (\text{A6})$$

Finally, the signal-to-noise ratio on the transit depth can be constructed by dividing the blocked photons N_{sp} by the standard deviation on that estimate:

$$\text{SNR}_T = \frac{N_s (R_p/R_s)^2}{\sqrt{(N_s + N_{bg})/n_{\text{out}} + N_s \left(1 - (R_p/R_s)^2 \right) + N_{bg}}}. \quad (\text{A7})$$

For secondary eclipse, the signal of interest is the number of photons missing when the planet is occulted by the star, which is measured assuming that the star is not varying. In this case, the out-of-eclipse photon fluence is measured as

$$N_{\text{out}} = (N_p + N_s + N_{bg})n_{\text{out}}, \quad (\text{A8})$$

where n_{out} is the time of measurement outside of eclipse in units of the eclipse duration, N_p is the total number of planet photons over an eclipse duration, and the sum of N_p , N_s and N_{bg} is the total number of photons counted over an eclipse duration. The in-eclipse photon fluence measured is

$$N_{ec} = N_s + N_{bg}, \quad (\text{A9})$$

which allows the planet photon counts to be estimated as

$$N_p = N_{\text{out}}/n_{\text{out}} - N_{ec}. \quad (\text{A10})$$

Again, analogous to the transit calculation, the noise term can be calculated by considering the variance on N_p given standard error propagation:

$$\sigma^2 = \left(\frac{\partial N_p}{\partial N_{\text{out}}} \right)^2 \sigma N_{\text{out}}^2 + \left(\frac{\partial N_p}{\partial N_{ec}} \right)^2 \sigma N_{ec}^2 \quad (\text{A11})$$

$$= \left(\frac{1}{n_{\text{out}}} \right)^2 N_{\text{out}} + (-1)^2 N_{ec} \quad (\text{A12})$$

where we have used the fact that N_{out} has a variance of N_{out} . Substituting in for N_{out} and N_{ec} gives:

$$\sigma^2 = \frac{(N_p + N_s + N_{bg})}{n_{\text{out}}} + N_s + N_{bg}. \quad (\text{A13})$$

Finally, the signal-to-noise ratio on the eclipse depth can be constructed by dividing the estimated planet photons by the standard deviation on that estimate:

$$\text{SNR}_E = \frac{N_p}{\sqrt{(N_p + N_s + N_{bg})/n_{\text{out}} + N_s + N_{bg}}}. \quad (\text{A14})$$

B. ATMOSPHERIC DETECTABILITY BY INSTRUMENT

Figures 13, 14, 15, 16, 17, 18, and 19, show the number of transits needed to detect the atmospheres of TRAPPIST-1 b, c, d, e, f, g, and h, respectively, as a function of both atmospheric compositions and JWST instrument/mode. The detection of an atmosphere requires $\langle \text{SNR} \rangle = 5$ on spectral features in the transmission spectrum.

C. BRIGHTNESS TEMPERATURES

Table 3 shows the brightness temperature of each [Lincowski et al. \(2018\)](#) TRAPPIST-1 atmospheric model in each of the JWST/MIRI photometric filters and the two warm *Spitzer* bands.

T-1b Transit : Detect Features with $\langle \text{SNR} \rangle = 5.0$

10 bar CO ₂	14	16	10	5	5	76	7	6	6	4	2
92 bar CO ₂	14	17	10	5	5	73	6	6	6	4	2
10 bar O ₂ outgassing	9	9	10	4	4	55	6	6	5	3	2
100 bar O ₂ outgassing	10	9	10	5	4	44	7	7	6	4	2
10 bar O ₂ desiccated	7	10	7	3	3	21	5	5	4	3	2
100 bar O ₂ desiccated	11	10	10	5	3	64	8	7	6	4	2
	NIRCam F322W2	NIRCam F444W	NIRSpec G140H	NIRSpec G235H	NIRSpec G395H	MIRI LRS	NIRISS SOSS substrip256	NIRISS SOSS substrip96	NIRSpec Prism sub512	NIRSpec Prism sub512s	NIRSpec Prism sub512 ngroup6

Figure 13. Number of TRAPPIST-1b transits necessary to rule out a featureless spectrum with $\langle \text{SNR} \rangle = 5$ for different atmospheric compositions and using different JWST instruments and modes.

T-1c Transit : Detect Features with $\langle \text{SNR} \rangle = 5.0$

10 bar CO ₂	27	32	20	8	9	>100	12	12	10	7	4
92 bar CO ₂	28	34	20	8	9	>100	12	12	10	7	4
10 bar Venus	>100	59	>100	40	30	>100	86	84	56	34	18
92 bar Venus	>100	51	>100	60	26	>100	>100	>100	76	46	22
10 bar O ₂ outgassing	18	18	18	6	7	100	11	10	9	6	3
100 bar O ₂ outgassing	19	17	23	9	7	64	16	15	11	7	4
10 bar O ₂ desiccated	16	19	17	6	5	51	11	11	9	5	3
100 bar O ₂ desiccated	26	18	22	11	7	>100	17	16	13	8	4
	NIRCam F322W2	NIRCam F444W	NIRSpec G140H	NIRSpec G235H	NIRSpec G395H	MIRI LRS	NIRISS SOSS substrip256	NIRISS SOSS substrip96	NIRSpec Prism sub512	NIRSpec Prism sub512s	NIRSpec Prism sub512 ngroup6

Figure 14. Number of TRAPPIST-1c transits necessary to rule out a featureless spectrum with $\langle \text{SNR} \rangle = 5$ for different atmospheric compositions and using different JWST instruments and modes.

T-1d Transit : Detect Features with $\langle \text{SNR} \rangle = 5.0$

10 bar CO ₂	15	17	10	4	5	87	7	6	6	4	2
92 bar CO ₂	14	17	10	4	5	84	6	6	5	3	2
10 bar Venus	>100	38	>100	51	21	>100	72	67	49	30	15
92 bar Venus	>100	59	>100	67	33	>100	>100	>100	79	48	24
10 bar O ₂ outgassing	10	10	10	4	4	51	7	6	6	4	2
100 bar O ₂ outgassing	8	8	8	4	4	28	6	6	5	3	2
10 bar O ₂ desiccated	9	10	9	4	3	31	6	6	5	3	2
100 bar O ₂ desiccated	13	9	10	5	4	48	8	7	6	4	2
	NIRCam F322W2	NIRCam F444W	NIRSpec G140H	NIRSpec G235H	NIRSpec G395H	MIRI LRS	NIRISS SOSS substrip256	NIRISS SOSS substrip96	NIRSpec Prism sub512	NIRSpec Prism sub512s	NIRSpec Prism sub512 ngroup6

Figure 15. Number of TRAPPIST-1d transits necessary to rule out a featureless spectrum with $\langle \text{SNR} \rangle = 5$ for different atmospheric compositions and using different JWST instruments and modes.

T-1e Transit : Detect Features with $\langle \text{SNR} \rangle = 5.0$

1 bar H ₂ O	88	46	>100	36	20	>100	85	80	41	25	13
1 bar H ₂ O cloudy	>100	60	>100	73	29	>100	>100	>100	81	49	23
10 bar CO ₂	53	60	54	17	17	>100	30	28	22	14	7
92 bar CO ₂	58	72	54	17	20	>100	30	28	23	14	8
10 bar Venus	>100	93	>100	69	45	>100	>100	>100	99	60	30
92 bar Venus	>100	>100	>100	69	50	>100	>100	>100	>100	62	31
10 bar O ₂ outgassing	59	38	87	25	16	>100	53	50	33	20	10
100 bar O ₂ outgassing	36	35	75	27	14	73	45	42	24	15	7
10 bar O ₂ desiccated	42	36	58	17	13	>100	35	33	23	14	8
100 bar O ₂ desiccated	67	36	64	29	16	>100	49	46	34	21	11
	NIRCam F322W2	NIRCam F444W	NIRSpec G140H	NIRSpec G235H	NIRSpec G395H	MIRI LRS	NIRISS SOSS substrip256	NIRISS SOSS substrip96	NIRSpec Prism sub512	NIRSpec Prism sub512s	NIRSpec Prism sub512 ngroup6

Figure 16. Number of TRAPPIST-1e transits necessary to rule out a featureless spectrum with $\langle \text{SNR} \rangle = 5$ for different atmospheric compositions and using different JWST instruments and modes.

T-1f Transit : Detect Features with $\langle \text{SNR} \rangle = 5.0$

10 bar CO ₂	45	52	58	15	14	>100	29	27	20	12	7
92 bar CO ₂	45	50	58	15	14	>100	28	27	20	12	7
10 bar Venus	73	59	>100	22	22	>100	60	57	36	22	12
92 bar Venus	78	61	>100	24	23	>100	64	60	38	23	12
10 bar O ₂ outgassing	54	31	98	24	14	>100	54	51	30	19	9
100 bar O ₂ outgassing	25	27	56	19	10	34	29	28	16	10	5
10 bar O ₂ desiccated	32	27	58	14	11	72	30	29	18	11	6
100 bar O ₂ desiccated	48	31	72	27	13	93	51	48	29	18	9
	NIRCam F322W2	NIRCam F444W	NIRSpec G140H	NIRSpec G235H	NIRSpec G395H	MIRI LRS	NIRISS SOSS substrip256	NIRISS SOSS substrip96	NIRSpec Prism sub512	NIRSpec Prism sub512s	NIRSpec Prism sub512 ngroup6

Figure 17. Number of TRAPPIST-1f transits necessary to rule out a featureless spectrum with $\langle \text{SNR} \rangle = 5$ for different atmospheric compositions and using different JWST instruments and modes.

T-1g Transit : Detect Features with $\langle \text{SNR} \rangle = 5.0$

10 bar CO ₂	46	49	72	16	14	>100	33	31	21	13	7
92 bar CO ₂	49	48	74	17	14	>100	34	32	22	14	7
10 bar Venus	60	54	>100	19	18	>100	49	46	29	18	9
92 bar Venus	70	58	>100	21	20	>100	56	52	33	20	11
10 bar O ₂ outgassing	58	34	>100	27	14	>100	69	66	34	21	10
100 bar O ₂ outgassing	24	29	41	17	11	31	21	20	13	8	4
10 bar O ₂ desiccated	31	26	73	15	11	60	33	31	18	11	6
100 bar O ₂ desiccated	42	30	93	28	13	69	56	53	27	17	8
	NIRCam F322W2	NIRCam F444W	NIRSpec G140H	NIRSpec G235H	NIRSpec G395H	MIRI LRS	NIRISS SOSS substrip256	NIRISS SOSS substrip96	NIRSpec Prism sub512	NIRSpec Prism sub512s	NIRSpec Prism sub512 ngroup6

Figure 18. Number of TRAPPIST-1g transits necessary to rule out a featureless spectrum with $\langle \text{SNR} \rangle = 5$ for different atmospheric compositions and using different JWST instruments and modes.

T-1h Transit : Detect Features with $\langle \text{SNR} \rangle = 5.0$

10 bar CO ₂	44	48	70	15	13	>100	31	30	20	13	7
92 bar CO ₂	46	46	69	16	13	>100	31	30	20	13	7
10 bar Venus	51	50	91	17	15	>100	38	36	24	15	8
92 bar Venus	57	52	93	18	15	>100	40	38	25	15	8
10 bar O ₂ outgassing	50	34	>100	25	13	79	58	55	30	19	9
100 bar O ₂ outgassing	21	28	30	15	10	26	17	16	11	7	4
10 bar O ₂ desiccated	26	24	56	13	9	48	26	25	15	9	5
100 bar O ₂ desiccated	29	26	63	20	10	44	34	33	18	11	6
	NIRCam F322W2	NIRCam F444W	NIRSpec G140H	NIRSpec G235H	NIRSpec G395H	MIRI LRS	NIRISS SOSS substrip256	NIRISS SOSS substrip96	NIRSpec Prism sub512	NIRSpec Prism sub512s	NIRSpec Prism sub512 ngroup6

Figure 19. Number of TRAPPIST-1h transits necessary to rule out a featureless spectrum with $\langle \text{SNR} \rangle = 5$ for different atmospheric compositions and using different JWST instruments and modes.

Table 3. Brightness temperatures in different photometric filters for different models.

Planet	Model	IRAC1	IRAC2	F560W	F770W	F1000W	F1130W	F1280W	F1500W	F1800W	F2100W	F2550W
		(K)	(K)	(K)	(K)	(K)	(K)	(K)	(K)	(K)	(K)	(K)
T-1b	10 bar CO ₂	498	328	432	384	340	356	330	291	315	362	430
	92 bar CO ₂	495	328	432	383	340	357	330	289	315	362	430
	100 bar O ₂ outgassing	500	388	372	396	379	432	385	305	355	381	346
	10 bar O ₂ outgassing	514	391	357	394	394	425	377	300	345	371	329
	100 bar O ₂ desiccated	425	375	390	387	389	404	376	306	368	408	364
	10 bar O ₂ desiccated	436	357	401	405	369	397	360	292	346	408	380
	10 bar CO ₂	445	292	385	328	304	326	295	250	275	315	386
	92 bar CO ₂	437	290	380	324	303	326	293	248	273	313	382
	100 bar O ₂ outgassing	434	337	325	346	312	390	343	266	325	345	308
	10 bar O ₂ outgassing	424	334	313	350	337	378	330	252	304	332	294
T-1c	100 bar O ₂ desiccated	387	325	330	328	333	339	327	272	325	342	310
	10 bar O ₂ desiccated	395	313	339	341	322	345	318	257	310	347	322
	10 bar Venus	427	292	373	318	300	320	296	272	282	313	376
	92 bar Venus	435	287	382	317	297	324	291	250	275	303	383
	10 bar CO ₂	384	256	337	274	269	295	260	219	239	272	340
	92 bar CO ₂	380	254	333	271	268	295	259	215	237	269	337
	100 bar O ₂ outgassing	370	290	280	301	264	352	295	227	290	305	270
	10 bar O ₂ outgassing	361	283	270	299	287	324	285	215	267	291	260
	100 bar O ₂ desiccated	356	281	278	274	280	279	280	239	282	284	260
	10 bar O ₂ desiccated	362	275	286	286	279	293	277	225	275	292	269
T-1d	10 bar Venus	326	258	240	230	230	233	233	227	231	239	243
	92 bar Venus	375	251	332	264	263	288	256	223	245	271	335
	10 bar CO ₂	339	230	297	235	247	272	232	193	208	237	301
	92 bar CO ₂	335	226	292	229	243	267	228	189	206	233	294
	100 bar O ₂ outgassing	305	236	244	259	231	301	245	203	253	265	245
	10 bar O ₂ outgassing	346	243	243	256	243	267	244	191	239	259	238
	100 bar O ₂ desiccated	341	250	244	238	242	239	246	214	251	243	226
	10 bar O ₂ desiccated	346	246	250	246	242	249	244	200	247	251	232
	10 bar Venus	303	217	213	203	204	204	202	192	204	206	211
	92 bar Venus	311	223	287	228	235	254	225	195	220	242	285
T-1e	1 bar H ₂ O	296	267	243	259	272	277	267	213	258	260	236
	1 bar H ₂ O cloudy	287	253	241	247	250	253	248	212	247	249	243
	10 bar CO ₂	277	201	260	200	221	235	200	172	185	206	263
	92 bar CO ₂	271	196	262	195	216	225	194	171	183	202	260
	100 bar O ₂ outgassing	229	209	218	219	202	234	208	192	221	224	222
	10 bar O ₂ outgassing	326	212	218	216	206	223	210	178	209	218	213
	100 bar O ₂ desiccated	268	225	228	216	210	209	219	192	227	213	194

Table 3 continued

Table 3 (continued)

Planet	Model	IRAC1	IRAC2	F560W	F770W	F1000W	F1130W	F1280W	F1500W	F1800W	F2100W	F2550W
		(K)	(K)	(K)	(K)	(K)	(K)	(K)	(K)	(K)	(K)	(K)
T-1g	10 bar O ₂ desiccated	298	222	229	223	210	216	218	184	227	219	200
	10 bar Venus	272	189	210	188	193	193	188	171	184	189	199
	92 bar Venus	247	197	239	199	211	218	196	177	195	210	237
	10 bar CO ₂	231	181	236	180	203	205	179	160	170	185	232
	92 bar CO ₂	229	177	240	175	200	197	174	158	167	181	231
	100 bar O ₂ outgassing	209	191	199	199	188	202	192	180	205	204	194
	10 bar O ₂ outgassing	312	195	202	194	187	199	191	166	188	192	191
	100 bar O ₂ desiccated	224	207	210	200	192	187	201	180	208	189	176
	10 bar O ₂ desiccated	276	205	211	205	192	192	200	174	209	195	178
	10 bar Venus	242	173	210	173	183	181	173	158	168	174	190
T-1h	92 bar Venus	226	182	222	181	200	199	177	165	176	191	217
	10 bar CO ₂	174	157	217	155	176	167	154	145	150	157	186
	92 bar CO ₂	175	154	206	151	174	162	151	143	147	153	182
	100 bar O ₂ outgassing	195	168	171	170	166	169	167	163	174	172	164
	10 bar O ₂ outgassing	296	181	184	170	165	167	170	150	165	164	160
	100 bar O ₂ desiccated	199	183	185	179	170	161	177	165	181	162	149
	10 bar O ₂ desiccated	253	184	188	183	171	164	179	160	186	167	150
	10 bar Venus	209	155	185	153	162	161	153	145	149	154	162
	92 bar Venus	189	159	195	156	185	169	146	145	144	161	187

NOTE—Table note 1